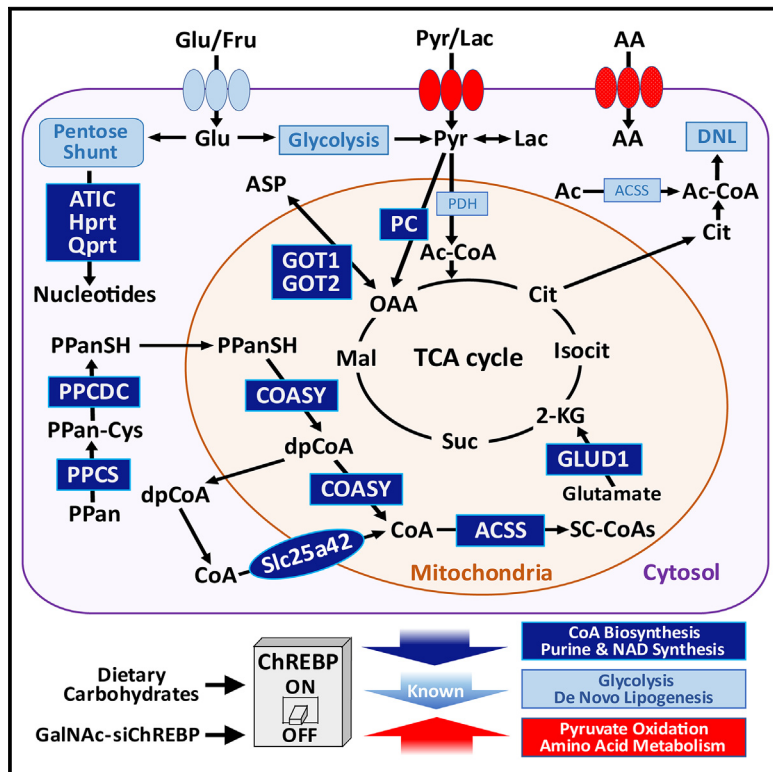


Integration of metabolomic and transcriptomic analyses reveals regulatory functions of the ChREBP transcription factor in energy metabolism

Graphical abstract



Authors

Jie An, Inna Astapova, Guofang Zhang, ..., Joseph Brozinick, Mark A. Herman, Christopher B. Newgard

Correspondence

chris.newgard@duke.edu

In brief

An et al. use an integrated metabolomic and transcriptomic approach in rats with liver-selective suppression of ChREBP to unveil metabolic functions of the transcription factor in multiple pathways, including nucleotide and CoA metabolism and amino acid and monocarboxylic acid transport.

Highlights

- The metabolic impact of chronic suppression of ChREBP in liver is reported
- Metabolomics and transcriptomics are applied to define ChREBP-dependent changes
- ChREBP drives metabolic changes beyond its role in carbohydrate and lipid metabolism
- Affected pathways include nucleotide and CoA metabolism and amino acid and pyruvate transport



Article

Integration of metabolomic and transcriptomic analyses reveals regulatory functions of the ChREBP transcription factor in energy metabolism

Jie An,^{1,7} Inna Astapova,^{2,7} Guofang Zhang,^{1,3} Andrew L. Cangelosi,¹ Olga Ilkayeva,^{1,3} Hannah Marchuk,¹ Michael J. Muehlbauer,¹ Tabitha George,¹ Joseph Brozinick,⁴ Mark A. Herman,^{2,6} and Christopher B. Newgard^{1,3,5,6,8,*}

¹Sarah W. Stedman Nutrition and Metabolism Center & Duke Molecular Physiology Institute, Duke University Medical Center, Durham, NC, USA

²Division of Endocrinology, Diabetes and Metabolism, Department of Medicine, Baylor College of Medicine, Houston, TX, USA

³Division of Endocrinology, Metabolism and Nutrition, Department of Medicine, Duke University Medical Center, Durham, NC, USA

⁴Eli Lilly Research Laboratories, Indianapolis, IN, USA

⁵Department of Pharmacology & Cancer Biology, Duke University Medical Center, Durham, NC, USA

⁶Senior author

⁷These authors contributed equally

⁸Lead contact

*Correspondence: chris.newgard@duke.edu

<https://doi.org/10.1016/j.celrep.2025.115278>

SUMMARY

The transcription factor carbohydrate response element binding protein (ChREBP) activates genes of glucose, fructose, and lipid metabolism in response to carbohydrate feeding. Integrated transcriptomic and metabolomic analyses in rats with GalNac-siRNA-mediated suppression of ChREBP expression in liver reveal other ChREBP functions. GalNac-siChREBP treatment reduces expression of genes involved in coenzyme A (CoA) biosynthesis, with lowering of CoA and short-chain acyl-CoA levels. Despite suppression of pyruvate kinase, pyruvate levels are maintained, possibly via increased expression of pyruvate and amino acid transporters. In addition, expression of multiple anaplerotic enzymes is decreased by GalNac-siChREBP treatment, affecting TCA cycle intermediates. Finally, GalNac-siChREBP treatment suppresses late steps in purine and NAD synthesis, with increases in precursors and lowering of end products in both pathways. In sum, our study reveals functions of ChREBP beyond its canonical roles in carbohydrate and lipid metabolism to include regulation of substrate transport, mitochondrial function, and energy balance.

INTRODUCTION

Excess consumption of diets enriched in fats and sugars leads to obesity and a myriad of metabolic derangements, including insulin resistance, glucose intolerance, type 2 diabetes, and hyperlipidemia. The effects of consumption of high-calorie diets on intermediary metabolism are orchestrated in part by transcription factors, including carbohydrate response element binding protein (ChREBP, encoded by the *Mlxip1* gene), sterol regulatory element binding protein (SREBP, also known as SREBF), and members of the peroxisome proliferator-activated receptor (PPAR) family and its co-activators such as PGC-1, each with the capacity to regulate genomic programs affecting diverse metabolic functions.

Our group has focused on the metabolic regulatory roles of ChREBP in the liver during feeding of high-calorie diets.^{1–5} Our prior studies and those of others have demonstrated that ChREBP is strongly activated by diets enriched in sucrose or fructose, resulting in induction of genes involved in glucose and fructose catabolism such as the glucose transporter *Slc2a2*

(encoding the GLUT2 protein) and the fructose transporter *Slc5* (GLUT5 protein), ketohexokinase (*Khk*), glucokinase regulatory protein (*Gckr*), triose kinase (*Tkfc*), glucose-6-phosphatase (*G6pc*), and pyruvate kinase liver/red blood cell isoform (*Pklr*), as well as genes involved in synthesis of lipids from glucose (*de novo* lipogenesis [DNL]) such as ATP-citrate lyase (*Acly*), acetyl-coenzyme A (CoA) carboxylase (*Acaca*), and fatty acid synthase (*Fasn*).^{1–11} Our recent work demonstrates that ChREBP also regulates genes involved in metabolism of branched-chain amino acids (BCAAs) in liver.¹² Refeeding of fasted rats with a diet high in fructose causes a large increase in expression of ChREBP, paralleled by increased expression of the transcript encoding branched-chain ketoacid dehydrogenase kinase (*Bckdk*), the enzyme that phosphorylates and inhibits activity of branched-chain ketoacid dehydrogenase (BCKDH), and a decrease in expression of *Ppm1k*, the phosphatase that dephosphorylates and activates BCKDH. Further, adenovirus-mediated overexpression of ChREBP in rat liver is sufficient to increase *Bckdk* and decrease *Ppm1k* transcript levels.¹²



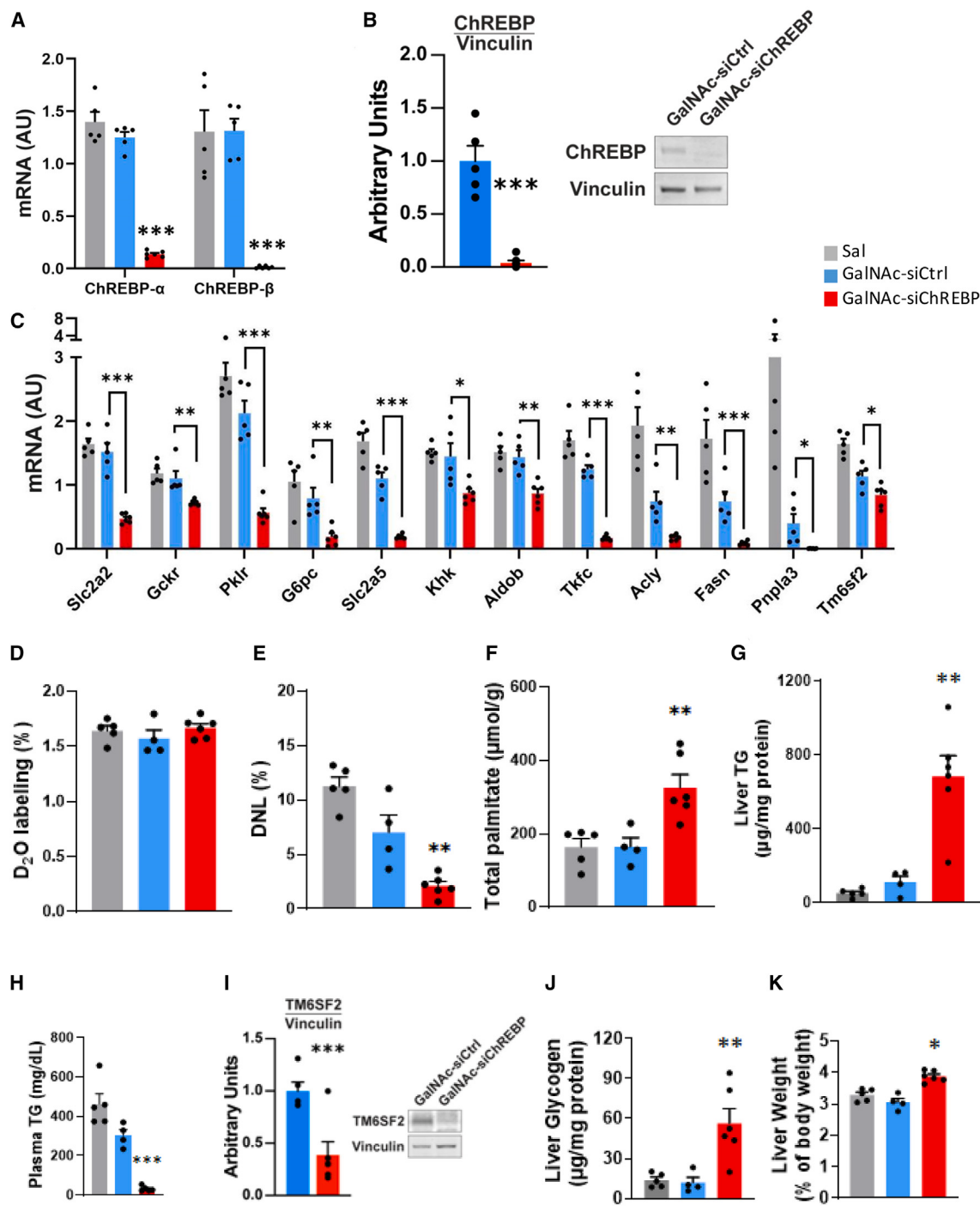


Figure 1. Effects of GalNAc-siChREBP on transcripts, metabolites, and de novo lipogenesis

Rats received multiple injections of GalNAc-siChREBP (red bars), GalNAc-siCtrl (blue bars), or saline (gray bars) over a 28-day period.

(A) Levels of transcripts encoding ChREBP- α and ChREBP- β measured by qPCR in liver.

(B) Levels of ChREBP protein shown by representative immunoblot (right) and densitometric analyses (left). The vinculin immunoblot is also presented in Figure 5D, as the same set of samples was used.

(C) Levels of transcripts encoding GLUT-2 (Slc2a2), glucokinase regulatory protein (Gckr), pyruvate kinase, liver isoform (Pklr), glucose-6-phosphatase (G6pc), GLUT-5 (Slc2a5), ketohexokinase (Khk), aldolase b (Aldob), triose kinase (Tkfc), ATP-citrate lyase (Acy), fatty acid synthase (Fasn), patatin-like phospholipase domain-containing protein 3 (Pnpla3), and transmembrane 6 superfamily 2 (Tm6sf2).

(D) D₂O enrichment of plasma water.

(E) Percent labeling of newly synthesized palmitate with D₂O in liver.

(legend continued on next page)

These recent findings suggest that ChREBP may regulate cellular and systemic metabolism in ways that transcend its well-studied effects on glucose and lipid metabolism to include other pathways. Also suggestive of alternative functions is the finding that despite potent activation of glycolytic flux by ChREBP, the liver is reported to shift from fatty acid oxidation (FAO) to pyruvate and lactate oxidation in response to global ChREBP knockout, associated with changes in energy charge and suppression of flux through the anaplerotic enzyme pyruvate carboxylase.¹³ However, the mechanisms and specific ChREBP transcriptional targets that might lead to these changes were not identified. Further studies to better understand the broader metabolic regulatory effects of ChREBP therefore seem warranted.

In the present study, we used ChREBP-specific small interfering RNAs (siRNAs) conjugated with *N*-acetylgalactosamine (GalNAc) to suppress expression of ChREBP in liver of rats fed a high-fat/high-sucrose (HF/HS) diet, then performed extensive metabolomic and transcriptomic profiling to reveal mechanisms by which ChREBP regulates cellular metabolism. The GalNAc conjugation method was chosen for its liver-selective transgene delivery and long-term modulation of gene expression.¹⁴ Using this technology, we achieved robust suppression of ChREBP expression in liver for 4 weeks, allowing us to gain a broad overview of the role of ChREBP in integration of hepatic fuel metabolism. This approach defined activities of ChREBP that extend beyond its canonical roles in regulation of carbohydrate and lipid metabolism to encompass diverse pathways of cellular fuel metabolism and energy balance, including CoA metabolism, purine and nicotinamide dinucleotide synthesis, and transport of amino acids and monocarboxylic acids.

RESULTS

GalNAc-siRNA achieves robust knockdown of ChREBP to affect markers of glucose and lipid metabolism

Consumption of foods and beverages high in added sugars, and particularly fructose, or conditions such as obesity that increase hepatic “reductive stress” and the abundance of hepatic carbohydrate metabolites, activate expression of ChREBP- α , which then acts upon an alternative promoter in the ChREBP gene to activate transcription of ChREBP- β , the more potent transcriptional activator among the two ChREBP isoforms.^{13,9,15} A cohort of obesity-prone (OP-CD) male Sprague-Dawley rats were fed an HF/HS diet for a period of 10 weeks beginning at 4 weeks of age. After this period of HF/HS feeding, the rats were divided into groups of 5–6 rats and injected subcutaneously with (1) an siRNA specific for ChREBP conjugated with GalNAc (GalNAc-

siChREBP); (2) a control, non-targeting siRNA conjugated with GalNAc (GalNAc-siCtrl); or (3) saline. Additional doses of each GalNAc-siRNA construct or saline were injected at 10, 18, and 25 days after the first treatment. Injection of GalNAc-siChREBP caused almost complete suppression of ChREBP- α and ChREBP- β transcripts in liver relative to the saline or GalNAc-siCtrl groups (Figure 1A), accompanied by a similarly potent suppression of ChREBP- α protein expression (Figure 1B). The reduction in ChREBP expression was accompanied by marked reductions in the hepatic expression of canonical ChREBP targets involved in glucose and fructose transport, glycolysis, glucose production, fructolysis, *de novo* lipogenesis, and packaging and export of very-low-density lipoprotein (VLDL) particles, consistent with prior studies (Figure 1C).^{1–11} Body weights were not different among rats in the three experimental groups (Figure S1A), and an intraperitoneal glucose tolerance test (IPGTT) performed at day 20 after onset of the GalNAc-siRNA treatments revealed no significant differences in glucose excursion (Figure S1B). Blood samples were also collected at the time of sacrifice (8 days after the IPGTT) and used for measurements of glucose and insulin levels. At that time point, no differences in blood glucose were observed (Figure S1C), whereas insulin levels were lowered by GalNAc-siChREBP treatment compared to the GalNAc-siCtrl-treated group (Figure S1D), resulting in a decrease in the homeostatic model assessment for insulin resistance (HOMA-IR), a measure of insulin sensitivity, in the GalNAc-siChREBP-treated group compared to the GalNAc-siCtrl-treated group (Figure S1E).

Effect of ChREBP suppression on DNL, hepatic fuel storage, lipid metabolism, and liver weight

All animal groups received a priming injection of D₂O and had D₂O added to their drinking water beginning 2 days before sacrifice to allow measurement of DNL in the liver.^{12,16} Enrichment of D₂O in plasma was equal in the three experimental groups (Figure 1D). GalNAc-siChREBP-treated rats exhibited a sharp decline in percent labeling of newly synthesized palmitate relative to either control group (Figure 1E). These findings are consistent with prior reports^{7,10} and with data in Figure 1C demonstrating reduced expression of key genes involved in DNL, such as Fasn and Acly, in response to ChREBP suppression. Interestingly, despite the decline in DNL, total palmitate levels were approximately doubled in livers from GalNAc-siChREBP-treated rats relative to either control group (Figure 1F). Supporting these findings, the level of newly labeled palmitate (measured as labeling of the M1 mass isotopomer of palmitate) decreased, whereas the level of unlabeled palmitate (measured as the M0 mass isotopomer of palmitate) increased, upon GalNAc-siChREBP treatment (Figures S1F and

(F) Total liver palmitate content (free and esterified).

(G) Liver triglyceride (TG) content.

(H) Plasma TG levels.

(I) Levels of TM6sf2 protein shown by representative immunoblot (right) and densitometric analysis (left) for four rats per group.

(J) Liver glycogen levels.

(K) Liver weights.

Data are the mean \pm standard error of the mean (SEM) for six independent liver samples for the GalNAc-siChREBP-treated group and 4–5 liver samples for the GalNAc-siCtrl-treated and saline-treated groups. Statistical analysis performed using one-way ANOVA followed by Tukey test (A, C–H, J, and K) or unpaired t test (B and I). Asterisks indicate differences in the GalNAc-siChREBP treatment group compared to the GalNAc-siCtrl group (B, C, I) or to either the GalNAc-siCtrl or saline group (A, D–H, J, K), with * p < 0.05, ** p < 0.01, and *** p < 0.005.

S1G). Overall, these data clearly demonstrate an increase in the total palmitate pool despite the decrease in new palmitate synthesis. In addition, GalNAc-siChREBP treatment caused a marked increase in liver triglyceride (TG) stores relative to either control group (Figure 1G), accompanied by a decrease in circulating TG (Figure 1H). The juxtaposition of increased hepatic TG with reductions in DNL and circulating TG is consistent with impaired hepatic VLDL packaging and secretion, as noted in other ChREBP loss-of-function models.^{4,10,17,18} This regulation of lipid export is thought to be mediated by transmembrane 6 superfamily 2 (TM6SF2) and/or microsomal TG transfer proteins (MTPPs).¹⁸⁻²⁰ Here, we confirmed that GalNAc-siChREBP treatment caused decreases in *Tm6sf2* mRNA levels (Figure 1C), as well as in TM6SF2 protein levels, as measured by immunoblot analysis (Figure 1I). GalNAc-siChREBP treatment also caused a significant increase in liver glycogen compared to either the GalNAc-siCtrl or saline-injected control groups (Figure 1J), consistent with downregulation of *G6pc* and *Pkr* in glycogen storage diseases.^{3,7,18,21} Thus, knockdown of ChREBP caused the liver to increase storage of two major fuels: fatty acids in the form of TG and glucose in the form of glycogen. Consistent with these findings, GalNAc-siChREBP treatment caused an increase in liver weight relative to either control group (Figure 1K).

Global transcriptomic effects of GalNAc-siChREBP treatment assessed by RNA-seq analysis

To gain insight into transcriptomic programs that may drive non-canonical actions of ChREBP, we performed RNA sequencing (RNA-seq) analysis on livers from HF/HS-fed rats injected with GalNAc-siChREBP, GalNAc-siCtrl, or saline. Principal-component analysis separated ChREBP knockdown from the two control groups (Figure 2A). However, the GalNAc-siCtrl control samples also separated from the saline control samples. Gene set enrichment analysis performed on rats treated with GalNAc-siCtrl compared to saline identified genes involved in cholesterol and other sterol biosynthetic processes as well as genes involved in lipid metabolism and lipid droplet organization (Data S1 and S2). These genes were enriched for targets of the transcription factor NR1I3, also known as constitutive androstane receptor β (CAR- β), which is responsive to a range of xeno-biotics including some sterols to regulate liver and systemic lipid metabolism.²² Consistent with this, *Nrl3* expression is reduced in livers from rats treated with GalNAc-siCtrl compared to saline (Data S2). Thus, treatment of animals with GalNAc siRNA may have “off-target” effects on lipid metabolism mediated in part through effects on CAR- β . These findings support a focused comparison of the GalNAc-siChREBP and GalNAc-siCtrl groups as the most rigorous approach for defining ChREBP-specific effects on metabolism going forward, as it controls for non-specific effects of the GalNAc-mediated siRNA delivery method. Therefore, metabolites, transcripts, or proteins that are different in GalNAc-siChREBP-treated versus GalNAc-siCtrl-treated rats are emphasized in the data presentation and discussion that follows.

We further investigated differences between the GalNAc-siChREBP-treated and GalNAc-siCtrl-treated rats by “volcano plot” analysis of our RNA-seq data (Figure 2B). In liver samples from rats treated with GalNAc-siChREBP compared to treatment

with GalNAc-siCtrl, ChREBP (*Mlxip1*) was the most significantly downregulated transcript, confirming the efficiency of our knockdown strategy (Figure 2B; Data S3). Other well-known ChREBP target genes¹⁻¹¹ involved in glucose and fructose catabolism, glucose production, and lipogenesis were also significantly downregulated in response to GalNAc-siChREBP treatment (Figure 1C; Data S3 and S4). ChREBP is known to regulate *Fgf21* expression,²³ and this gene was significantly suppressed in response to GalNAc-siChREBP treatment as expected (annotated as ENSRNOG00000020990 in the rat RNA-seq dataset summarized in Data S3). Gene set enrichment analysis also identified downregulation of key regulators of liver metabolism such as SREBF1, HNF4A, and HIF1A (Figures 2C and 2D). We also found evidence for regulation of networks unrelated to core intermediary metabolic pathways. This included effects of ChREBP knockdown to increase expression of gene sets involved in extracellular matrix remodeling, inflammation, and immune responses (Figures 2C and 2D). Differentially regulated genes involved in these processes were enriched for targets of the transcription factors RELA and NFKB1, which are known to regulate stress and inflammatory responses. These results are consistent with a role for ChREBP in mediating the adaptive response to overnutrition.^{1,2}

Finally, the GalNAc-siRNA approach used in this study was chosen for liver-selective delivery of the siRNA constructs based on the high affinity of GalNAc for the asialoglycoprotein receptor, which is preferentially and abundantly expressed in liver.^{14,24} Supporting the specificity of this approach, we found no change in expression of ChREBP- α or its key target genes *Fasn*, *Acaca*, or *Acly* in adipose tissue, an important alternative site of ChREBP expression (Figure S1H).

Alterations in hepatic lipid metabolism in response to GalNAc-siChREBP treatment

GalNAc-siChREBP treatment caused a decrease in circulating non-esterified fatty acids (NEFAs) (Figure 3A), accompanied by an approximate 2.5-fold increase in circulating β -hydroxybutyrate and total ketone levels compared to the GalNAc-siCtrl-treated group (Figure 3B). GalNAc-siChREBP treatment did not affect circulating glycerol levels (Figure 3C), indicating that adipose tissue lipolysis was not impaired. The fall in circulating NEFAs, increases in liver TG and total palmitate, and increases in circulating ketones in the GalNAc-siChREBP group suggests increased hepatic fatty acid uptake and oxidation in response to hepatic ChREBP suppression. To further explore this idea, we used targeted tandem mass spectrometry to find clear increases in a set of even-chain acylcarnitines produced by FAO in liver of GalNAc-siChREBP-treated rats compared to the two control groups (see heatmap in Figure 3D and absolute values in Data S5). This included intermediates produced in each round of the β -oxidation spiral from palmitate or oleate, including C18:1, C16:0, C16:1, C14:0, C14:1, and C12:0 acylcarnitines, which increased by 3.4- to 4.2-fold in livers of GalNAc-siChREBP-treated compared to GalNAc-siCtrl-treated rats, as well as a set of hydroxylated species of similar chain length thought to be generated by the individual FAO enzymes.²⁵ In addition, GalNAc-siChREBP treatment caused a 1.9-fold increase in β -hydroxybutyryl (C4-OH) carnitine, a marker of FAO

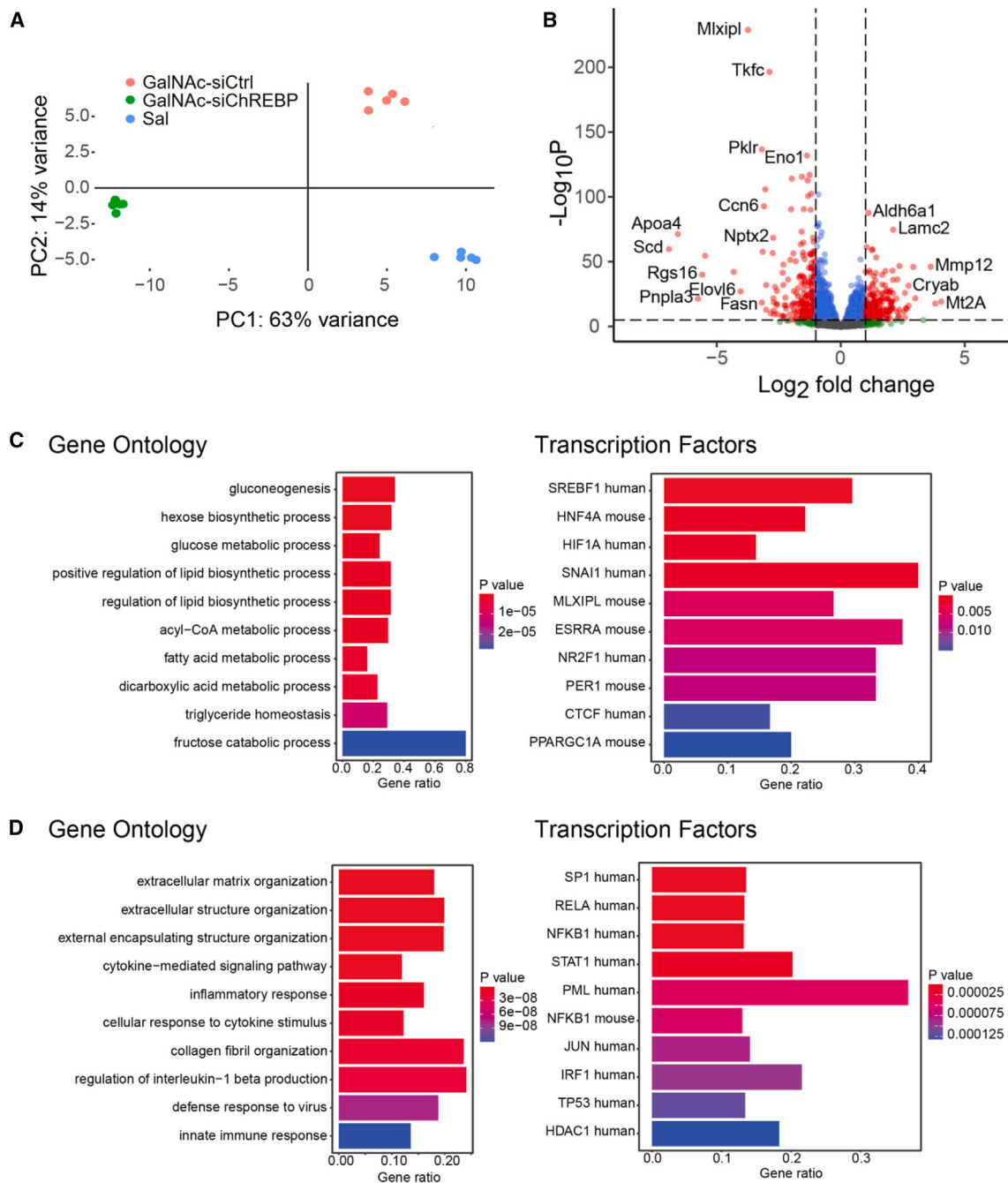


Figure 2. RNA-seq analysis

(A) Principal-component plot for GalNAc-siCtrl-treated (red dots), GalNAc-siChREBP-treated (green dots), and saline-treated (blue dots) rats. Each dot represents an individual animal.

(B) Volcano plot depicting differentially expressed genes in livers from GalNAc-siChREBP- versus GalNAc-siCtrl-treated animals.

(C) Pathway analysis showing the top ten Gene Ontology and transcription factor gene sets downregulated in livers of GalNAc-siChREBP-treated versus GalNAc-siCtrl-treated rats. Color is indicative of p value, and gene ratio corresponds to the fraction of genes in the gene set that contributed to enrichment.

(D) Pathway analysis showing the top ten Gene Ontology and transcription factor gene sets upregulated in livers of GalNAc-siChREBP-treated versus GalNAc-siCtrl-treated rats.

See [Data S1](#), [S2](#), [S3](#), and [S4](#) for supporting data.

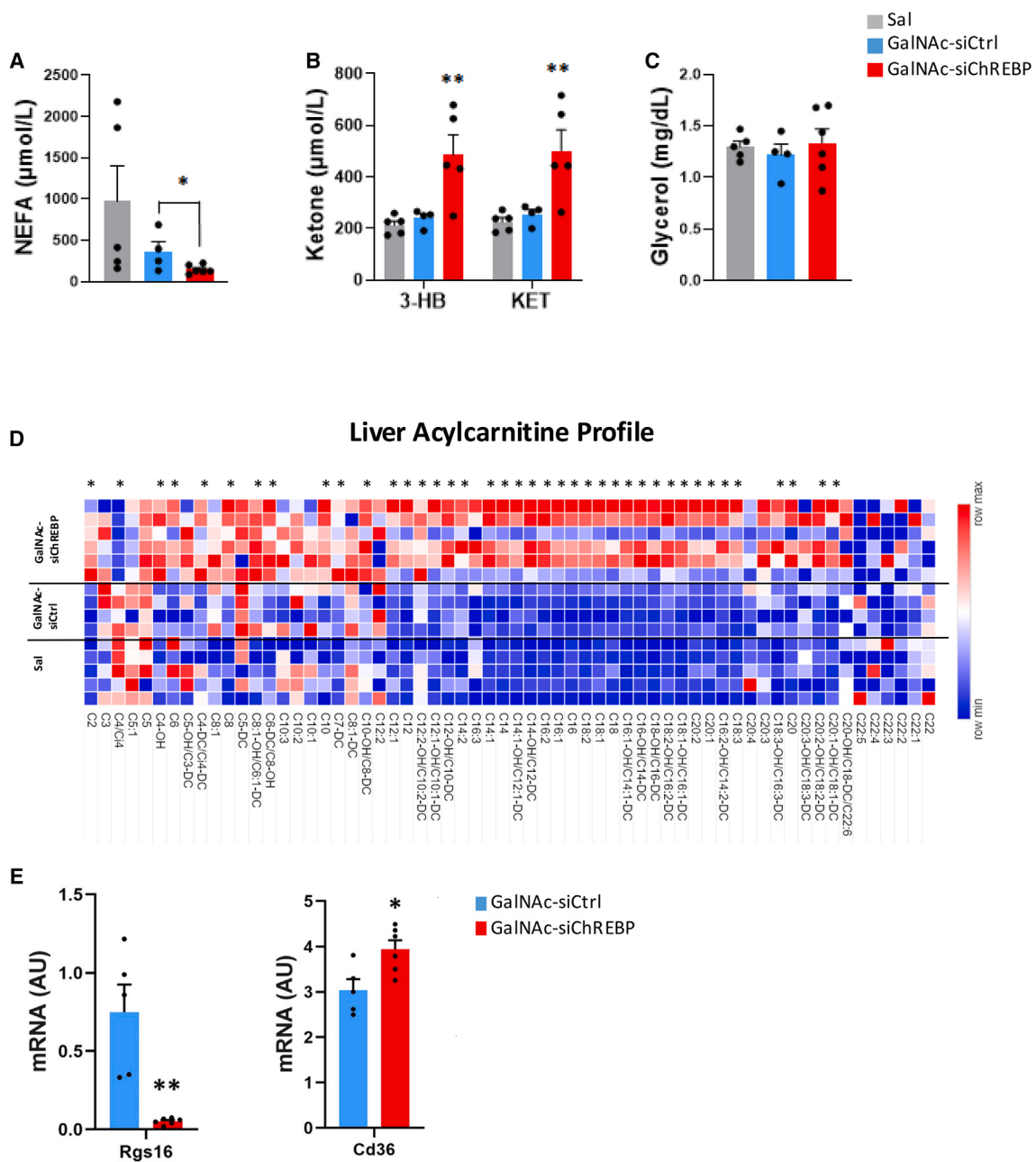


Figure 3. Effects of GalNAc-siChREBP on indices of lipid metabolism in plasma and liver

(A) Plasma non-esterified fatty acid (NEFA) levels.

(B) Plasma β -hydroxybutyrate (3-HB) and total ketone (KET) levels.

(C) Plasma glycerol levels.

(D) Levels of individual acylcarnitines in liver. Heatmap generated using Morpheus software (<https://software.broadinstitute.org/morpheus>). See Data S5 for acylcarnitine levels in individual rats.

(E) qPCR analysis of Rgs16 (left) and CD36 (right).

Data are the mean \pm SEM for six independent liver samples for the GalNAc-siChREBP-treated group and 4–5 liver samples for the GalNAc-siCtrl-treated and saline-treated groups. Statistical analysis performed using one-way ANOVA followed by Tukey test (A–D) or unpaired t test (E). Asterisks indicate differences in the GalNAc-siChREBP treatment group compared to the GalNAc-siCtrl group (E) or to either the GalNAc-siCtrl or saline group (A–D), with * $p < 0.05$ and ** $p < 0.01$.

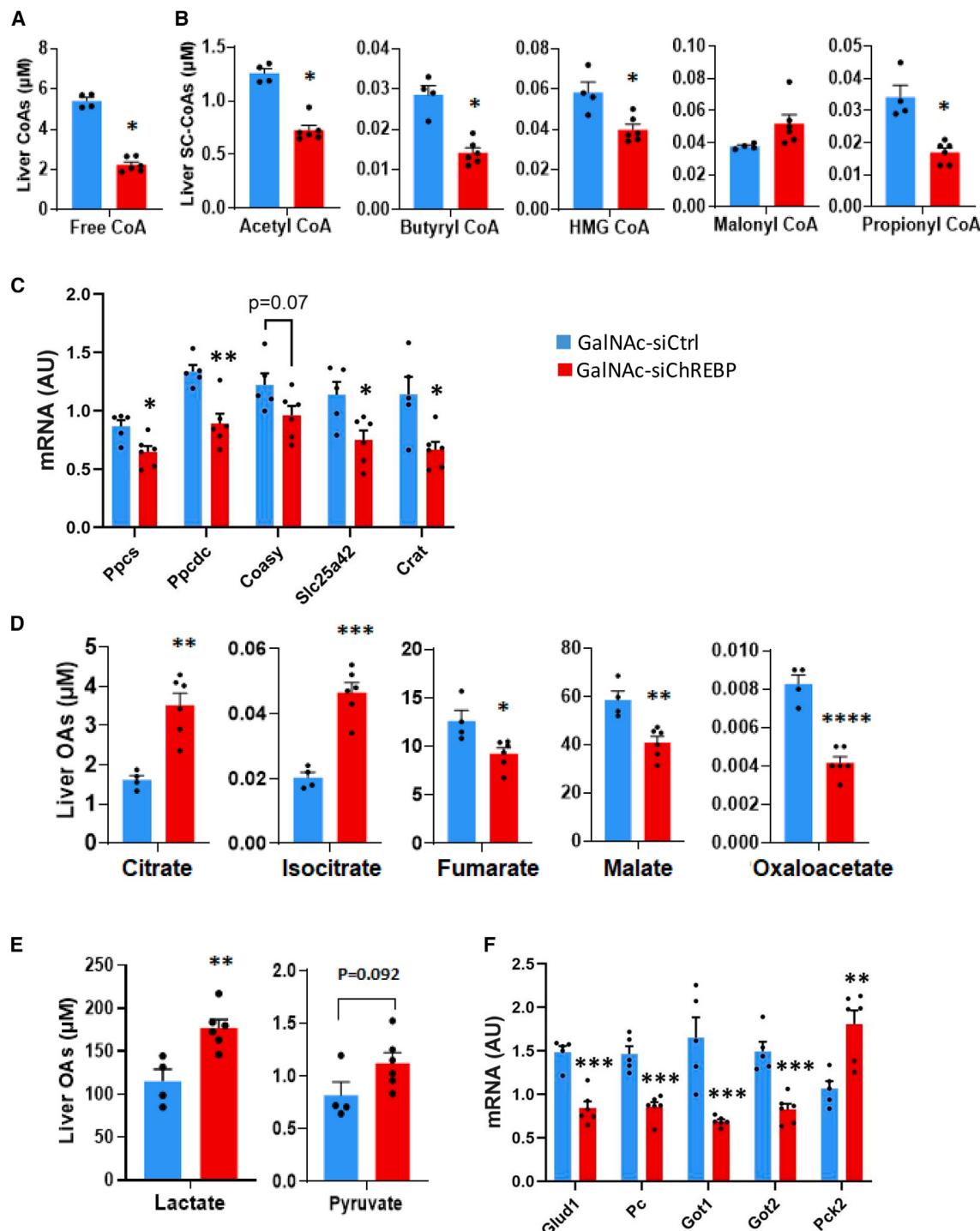


Figure 4. Effects of GalNAc-siChREBP on indices of acyl-CoA and TCA cycle metabolism in liver

(A) Free coenzyme A (CoA) levels in liver.

(B) Levels of short-chain acyl-CoA intermediates in liver.

(C) Expression of transcripts involved in metabolism of CoA and acyl-CoAs measured by qPCR, including phosphopantothenoylcysteine synthetase (Ppcsc), phosphopantothenoylcysteine decarboxylase (Ppcdc), CoA synthase (CoAsy), the mitochondrial CoA transporter (Slc25a), and carnitine O-acetyltransferase (Crat).

(D) Levels of TCA cycle intermediates in liver.

(E) Lactate and pyruvate levels in liver.

(legend continued on next page)

to ketones,²⁶ as well as a 1.7-fold increase in acetyl (C2) carnitine.

RNA-seq identifies genes involved in altered lipid handling in response to ChREBP knockdown

In light of the foregoing changes in indices of fatty acid metabolism, we used our RNA-seq dataset to identify changes in expression of transcripts encoding enzymes involved in FAO. Some, but not all enzymes of the mitochondrial FAO pathway were upregulated in response to GalNAc-siChREBP treatment, including acyl-CoA dehydrogenases *Acadl1* (very long chain; 1.4-fold increase, *padj* = 10^{-10}), *Acadl* (long chain; 1.2-fold increase, *padj* = 1×10^{-6}), enoyl-CoA hydratase *Echs1* (1.2-fold increase, *padj* = 7.7×10^{-5}), 3-hydroxyacyl-CoA dehydrogenase *Hacd2* (1.1-fold increase, *padj* = 0.002), and β -ketothiolase *Hadhb* (1.1-fold increase, *padj* = 0.086) (Figure S2A). Interestingly, medium-chain ACAD (*Acadm*) expression did not change in response to ChREBP suppression, while expression of short-chain ACAD (*Hadhd*, also known as SCHAD) decreased sharply (1.6-fold decrease, *padj* = 2.9×10^{-30}) (Figure S2A). Although the increases in expression of individual FAO genes may appear modest, small but concerted changes in multiple enzymes across pathways have been shown previously to have significant effects on pathway activities.²⁷ In contrast to these effects on transcripts encoding mitochondrial FAO enzymes, transcripts encoding enzymes of peroxisomal FAO were coordinately downregulated in livers of GalNAc-siChREBP-treated compared to GalNAc-siCtrl-treated rats, including acyl-CoA oxidase-1 *Acox1* (1.3-fold decrease, *padj* = 8.3×10^{-11}), D-bifunctional protein D-BP (*Hsd17b4*) (1.2-fold decrease, *padj* = 1.5×10^{-8}), and both isoforms of acyl-CoA acyltransferase 1 ACCA1 (*Acaa1a*, 1.8-fold decrease, *padj* = 2.9×10^{-48} ; *Acaa1b*, 1.9-fold decrease, *padj* = 1.3×10^{-10}) (Figure S2A). Suppression of ChREBP expression caused sharp downregulation of regulator of G protein 16 (*Rgs16*), a G protein that suppresses FAO (Figure 3E),²⁸ while increasing expression of the *Cd36* fatty acid transporter (Figure 3E) and decreasing levels of the *Tm6sf2* transcript and protein (Figures 1C and 1I), potentially contributing to the increase in hepatic palmitate and TG levels as reported in Figures 1 and S1. Altogether, these transcriptomic changes suggest that ChREBP suppression activates influx of circulating fatty acids (via upregulation of CD36) to increase FAO (via downregulation of Rgs16 and induction of the core enzymes of mitochondrial FAO), resulting in increases in circulating ketones and hepatic fatty-acid-derived acylcarnitines. The increases observed in a wide set of fatty-acid-derived acylcarnitine species reported in Figure 3 could reflect increased entry of fatty acids into the β -oxidation spiral, but an inadequate capacity to fully oxidize the intermediates to CO₂ in the tricarboxylic acid (TCA) cycle, as has been previously described in skeletal muscles of rodents fed on high-calorie diets.²⁹ This interpretation could be consistent with a prior study reporting suppression

of FAO in livers of mice with global ChREBP knockout, measured indirectly by ¹³C-NMR analysis of glutamate labeling.¹³

Analysis of short-chain acyl-CoA and free CoA

Seeking to expand our understanding of metabolic effects of ChREBP manipulation, we applied a targeted metabolomics panel for CoA and CoA-modified metabolic intermediates.³⁰ We unexpectedly observed a striking decrease in free CoA levels in GalNAc-siChREBP-treated rats compared to GalNAc-siCtrl-treated controls (Figure 4A). This was accompanied by marked reductions in several short-chain acyl-CoA metabolites, including acetyl-CoA, butyryl-CoA, 3-hydroxy-3 methylglutaryl (HMG)-CoA, and propionyl-CoA, but not the lipogenic precursor and CPT1 regulator malonyl-CoA (Figure 4B).

These findings led us to query our RNA-seq dataset for genes involved in CoA biosynthesis and metabolism of short-chain acyl-CoA metabolites. Three transcripts encoding enzymes of CoA synthesis from pantothenic acid were significantly reduced by GalNAc-siChREBP treatment: phosphopantothenoylcysteine synthetase (*Ppc*; 1.4-fold decrease, *padj* = 5.5×10^{-4}), phosphopantothenoylcysteine decarboxylase (*Ppcdc*; 1.4-fold decrease, *padj* = 6.6×10^{-5}), and CoA synthase (*Coasy*; 1.3-fold decrease, *padj* = 5.3×10^{-13}), all confirmed by qPCR (Data S3; Figure 4C). GalNAc-siChREBP treatment also resulted in reduced expression of the transcript encoding the mitochondrial CoA transporter (*Slc25a42*, 1.4-fold decrease, *padj* = 4.4×10^{-10}), also confirmed by qPCR (Figure 4C). In addition, the transcript encoding carnitine O-acetyltransferase (*Crat*) was decreased by GalNAc-siChREBP treatment (1.9-fold decrease, *padj* = 0.00049), confirmed by RT-PCR (Figure 4C). CRAT catalyzes the reversible conversion of free CoA + short-chain acylcarnitines to short-chain acyl-CoAs + carnitine. We hypothesize that the decreases observed in multiple short-chain acyl-CoA metabolites (Figure 4B) may be driven by the strong decrease in the free CoA pool and the reduction in CRAT activity. These factors may also explain how acetyl-CoA levels fall (Figure 4B) while acetylcarnitine (C2) levels increase (Figure 3D) in GalNAc-siChREBP-treated relative to GalNAc-Ctrl-treated rats, as conversion of acetylcarnitine to acetyl-CoA would be impaired by low CoA levels and reduced CRAT activity. The lack of decrease in malonyl-CoA levels could be related to its lower rate of utilization for DNL (Figure 1), thus offsetting the decrease in expression of the known ChREBP target gene and malonyl-CoA synthesizing enzyme acetyl-CoA carboxylase (*Acaca*) at both the transcript (Data S3) and protein (Figure S2C) levels.

Analysis of TCA cycle intermediates

Our finding of reduced levels of CoA and expression of CoA synthetic enzymes points to previously unanticipated changes in mitochondrial fuel metabolism resulting from ChREBP knockdown. Burgess et al. previously reported that global ChREBP

(F) Expression of transcripts involved in liver anaplerosis measured by qPCR, including glutamate dehydrogenase (*Glud1*), pyruvate carboxylase (*Pc*), both forms of aspartate transaminase (*Got1* and *Got2*), and the mitochondrial isoform of PEPCK (*Pck2*). Data are the mean \pm SEM for six independent liver samples for the GalNAc-siChREBP-treated group and 4–5 liver samples for the GalNAc-siCtrl-treated group. Statistical analysis performed using unpaired t test or multiple t test. Asterisks indicate significant differences in the GalNAc-siChREBP treatment group compared to the GalNAc-siCtrl group, with **p* < 0.05, ***p* < 0.01, ****p* < 0.001, and *****p* < 0.0001. Metabolite levels for individual rat livers are presented in Data S5.

knockout in mice results in reduced hepatic glucose catabolism but increased lactate and pyruvate oxidation to maintain energy balance in the face of impaired FAO.¹³ They also reported an increase in pyruvate dehydrogenase enzymatic activity without a change in pyruvate dehydrogenase (PDH) protein amount and a fall in expression of the PDK3 isoform, an inhibitory PDH kinase.¹³ Here, we found either a modest decrease or no change in expression of transcripts encoding a subset of PDH component subunits (*Pdha1*, *Pdhx*, and *Dlat*), with decreases in the levels of the transcript encoding PDHB (reduced 2.0-fold, *padj* = 2.6×10^{-14}) and the predominant PDH kinase *Pdk4* (reduced 2-fold, *padj* = 8.7×10^{-8}) and a trend for increase in expression of *Pdk3* (Figure S2B). We also measured phosphorylated and total PDHA protein levels, with no changes in either observed in response to GalNAc-siChREBP treatment (Figure S2C). We used targeted gas chromatography-mass spectrometry to measure a panel of organic acids/TCA cycle intermediates³¹ and found increases in hepatic citrate and isocitrate levels in GalNAc-siChREBP compared to GalNAc-siCtrl-treated rats, coupled with decreased levels of the more distal TCA cycle intermediates fumarate, malate, and oxaloacetate (Figure 4D). Pyruvate levels trended to increase (*p* = 0.09) in the GalNAc-siChREPB-treated rats, whereas lactate levels were significantly increased (Figure 4E). Overall, the noted increases in pyruvate and lactate levels in the absence of changes in total amount or phosphorylation of PDHA may be sufficient to drive an increased rate of pyruvate and lactate oxidation in response to ChREBP knockdown, consistent with the prior study.¹³

The fall in oxaloacetate and acetyl-CoA levels and increase in citrate and isocitrate that we report in Figure 4 could be consistent with an increase in acetyl-CoA and oxaloacetate consumption through the PDH, citrate synthase, and isocitrate dehydrogenase reactions to form citrate and isocitrate. Another possible contributor to the rise in the citrate and isocitrate pools in livers of GalNAc-siChREBP-treated rats could be the decrease in *Acy* and *Acaca* expression that occurs in response to ChREBP suppression (Figure 1C; Data S3), limiting the use of citrate to form acetyl-CoA and malonyl-CoA as substrates for DNL. This framework raises the question of the source of pyruvate for driving PDH flux, especially in light of the sharp decrease in pyruvate kinase expression (Figure 1C). To investigate this, we examined the expression of the family of monocarboxylic acid carriers, including five isoforms known to be pyruvate and lactate transporters, and found increases in transcript levels for three of the five, namely *Slc16a3*, *Slc16a4*, and *Slc16a7* (1.2-fold increase, *padj* = 0.0004; 1.2-fold increase, *padj* = 0.004; 1.7-fold increase, *padj* = 0.009, respectively), with no significant change in expression of a fourth member, *Slc16a1*, and a decrease in expression of the fifth member, *Slc16a11* (Figure S2D). Among other members of the SLC16a family, a transporter of aromatic amino acids, *SLC16a10*, was significantly increased, whereas the thyroid transporter *Slc16a2* was significantly decreased, whereas other family members (*Slc16a6*, *Slc16a9*, *Slc16a12*, *Slc16a13*) exhibited no significant change in expression (Figure S2E), highlighting the selective pattern of increased expression of a subset of pyruvate/lactate transporters in our dataset. Interestingly, the transcripts for lactate dehydrogenase a (LDHa) and glutamate/pyruvate transaminase 2 (GPT2) were

both decreased in response to GalNAc-siChREBP treatment (2.3-fold decrease, *p* = 1.07×10^{-31} and 1.5-fold decrease, *p* = 6.4×10^{-5} , respectively), as confirmed by qPCR (Figure S2F), possibly serving as an additional mechanism for preserving the pyruvate pool for oxidation.

A surprising finding is that the clear increases in citrate and isocitrate levels in livers of GalNAc-siChREBP-treated rats occurred despite induction of 2-ketoglutarate dehydrogenase expression (*Ogdh*, the enzyme that converts citrate to succinyl-CoA; 0.52-fold increase, *padj* = 6.9×10^{-24}). We interpret this to mean that the marked depletion of free CoA in GalNAc-siChREBP-treated rats limits its supply as a co-factor for the 2-oxoglutarate dehydrogenase (OGDH) reaction, contributing to accumulation of the proximal metabolites citrate and isocitrate even in the face of induction of the *Ogdh* gene, accompanied by decreased levels of the more distal TCA cycle metabolites succinate, fumarate, and malate.

These data prompted examination of the expression of key anaplerotic enzymes that feed carbon into the TCA cycle. All those examined were found to be strongly downregulated in livers from GalNAc-siChREBP-treated compared to GalNAc-siCtrl-treated rats, including glutamate dehydrogenase (*GLUD1*, *padj* = 1.34×10^{-15}), pyruvate carboxylase (*Pc*, *padj* = 2.99×10^{-21}), and both forms of aspartate transaminase (*GOT1*, *padj* = 1.5×10^{-12} , and *GOT2*, *padj* = 1.6×10^{-109}), all confirmed by qPCR (Figure 4F). This raises the question of how the livers of GalNAc-siChREBP-treated rats generate anaplerotic substrates for formation and expansion of the citrate and isocitrate pools as shown in Figure 4D. One possibility is the mitochondrial isoform of PEPCK (PCK2), which normally generates phosphoenolpyruvate (PEP) from oxaloacetate and guanosine triphosphate (GTP) in an irreversible reaction but which has been shown to catalyze oxaloacetate formation from PEP in bacteria lacking pyruvate kinase.³² A role for PCK2 to catalyze this reaction has also been suggested in mammalian cells.³³ In a study in which an adenovirus vector was used to express PCK2 in PCK1 knockout mice, an increase in TCA cycle flux was observed, but conversion of PEP to oxaloacetate was not directly measured.³⁴ The near-complete silencing of pyruvate kinase expression in response to GalNAc-siChREBP treatment (Figure 1C) may be linked to the robust induction of *Pck2* (2.0-fold increase, *p* = 1.4×10^{-33}), as confirmed by qPCR (Figure 4F). Interestingly, in contrast to the dramatic increase in the *Pck2* transcript, expression of the cytosolic *Pck1* isoform was not affected by ChREBP suppression (Data S3).

Effects of ChREBP on amino acid metabolism

Targeted profiling of hepatic amino acid levels revealed significant decreases in hepatic Gly, Leu/Ile (a combined measure of leucine and isoleucine), Asx (a combined measure of aspartate and asparagine), ornithine, and Tyr levels in livers of GalNAc-siChREBP-treated compared to GalNAc-siCtrl-treated animals (Figure 5A). In addition, RNA-seq analysis revealed induction of multiple transcripts encoding plasma membrane amino acid transporters in GalNAc-siChREBP-treated animals, including the large neutral amino acid/BCAA carrier (LAT1, *Slc7a5*), the alanine/taurine carrier (*Slc6a6*), the glutamate transporter

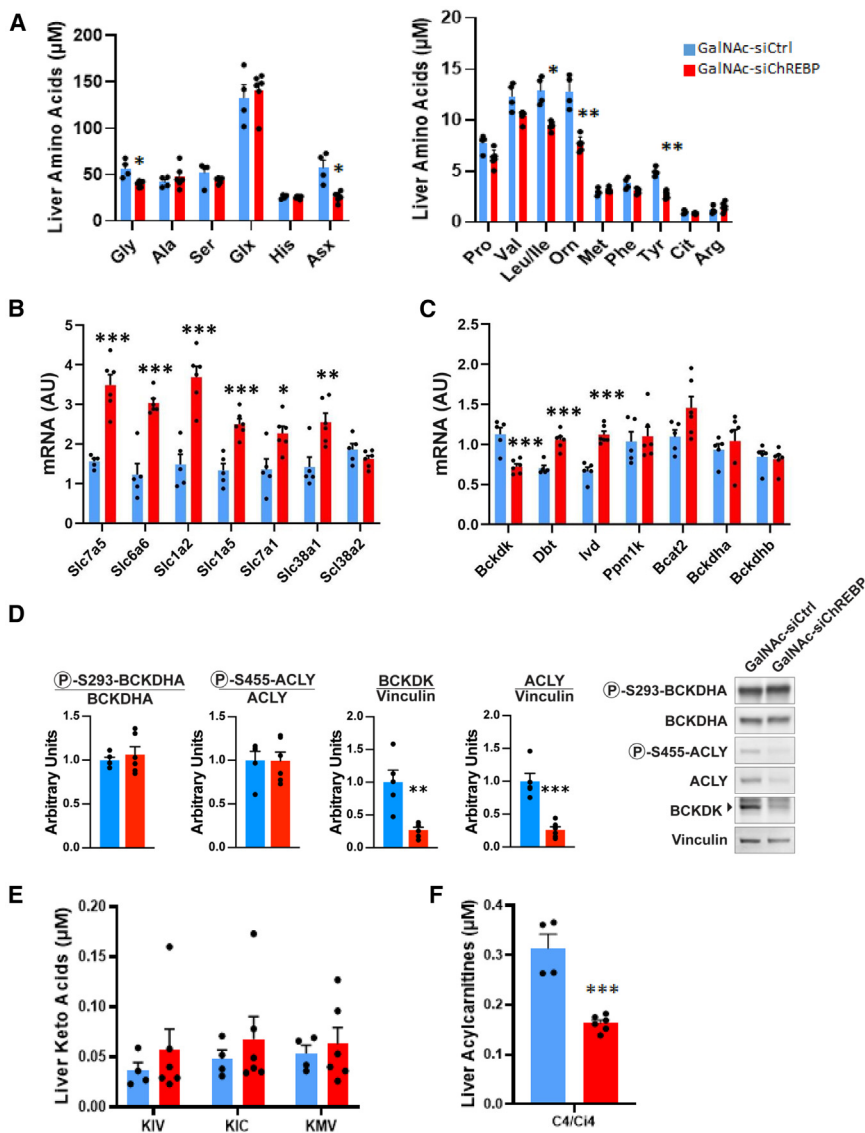


Figure 5. Effects of GalNAc-siChREBP on indices of amino acid metabolism

(A) Liver amino acid levels.

(B) qPCR analysis of transcripts encoding amino acid transporters.

(C) Regulation of transcripts encoding proteins involved in BCAA catabolism, including branched-chain ketoacid dehydrogenase kinase (*Bckdk*), lipoamide acyltransferase (*Dbt*), isovaleryl-CoA dehydrogenase (*Ivd*), BCKDH phosphatase (*Ppm1k*), branched-chain aminotransferase-2 (*Bcat2*), branched-chain ketoacid dehydrogenase α subunit (*Bckdha*), and branched-chain ketoacid dehydrogenase β subunit (*Bckdhb*).

(D) Representative immunoblot (right) and densitometric quantification (left) of phosphorylated (P-S293-BCKDHA) and total branched-chain ketoacid dehydrogenase A (BCKDHA), phosphorylated (P-S455-ACLY) and total ATP-citrate lyase (ACLY), branched-chain ketoacid dehydrogenase kinase (BCKDK), and vinculin as a loading control. The vinculin immunoblot is also shown in Figure 1B, as the same set of samples was used.

(E) Levels of the branched-chain ketoacids ketosovalerate (KIV), ketoisocaproate (KIC), and ketomethylvalerate (KMV).

(F) Levels of C4/Ci4 acylcarnitine in liver.

Data are the mean \pm SEM for six independent rats/liver samples for the GalNAc-siChREBP-treated group and 4–5 rats/liver samples for the GalNAc-siCtrl-treated group. Statistical analysis performed using unpaired t test or multiple t test. Asterisks indicate differences in the GalNAc-siChREBP treatment group compared to the GalNAc-siCtrl group, with * $p < 0.05$, ** $p < 0.01$, and *** $p < 0.001$. Metabolite levels for individual rat livers are presented in Data S5.

(*Slc1a2*), the neutral amino acid transporter for Thr, Ser, Cys, Ala, and Gln (ASCT2), *Slc1a5*, the arginine/histidine transporter (*Slc7a1*), and the glutamine transporter (*Slc38a1*), all confirmed by qPCR (Figure 5B). Of note, the transcript encoding the sodium-coupled neutral amino acid transporter 2 (SNAT2, *Slc38a2*), previously reported by another group to be suppressed by overexpression of ChREBP,³⁵ was not significantly altered by GalNAc-siChREBP treatment in our studies (Figure 5B). In the prior study, chromatin immunoprecipitation (ChIP) was used to demonstrate binding of ChREBP to the SNAT2 promoter *in vivo*, but only in isolated hepatocytes, and effects of ChREBP suppression *in vivo* were not described. Overall, the observed increases in amino acid transporter expression, coupled with the decreases in levels of multiple liver amino acids, suggests that ChREBP suppression may activate amino acid catabolism as an alternative energy source, possibly including increased use of glycine for pyruvate and ketone production.³⁶

leading to amino acid depletion accompanied by a compensatory upregulation of hepatic amino acid transporters to offset this decline.

We also examined the impact of GalNAc-siChREBP treatment on expression of a broad set of genes involved in BCAA catabolism. In agreement with our recent finding that overexpression of ChREBP- β increases expression of *Bckdk* in liver,¹² administration of GalNAc-siChREBP decreased *Bckdk* mRNA levels, which would be expected to result in increased BCKDH activity and BCAA catabolism (Figure 5C). Consistent with this model, ChREBP knockdown caused an increase in expression of the E2 component (lipoamide acyltransferase, *Dbt*) of the BCKDH complex, as well as an increase in the transcript encoding isovaleryl-CoA dehydrogenase (*Ivd*), the third enzyme in catabolism of leucine (Figure 5C). Other genes involved in BCAA metabolism including *Ppm1k*, *Bcat2*, *Bckdha*, and *Bckdhb* were not significantly affected by ChREBP knockdown (Figure 5C). Treatment with GalNAc-siChREBP caused a 75% decrease in BCKDK protein levels relative to GalNAc-siCtrl-treated rats but had no effect on BCKDH phosphorylation (Figure 5D). Also, GalNAc-siChREBP treatment reduced phospho-S455 ACLY levels, but

this effect could be accounted for by a reduction in total ACLY protein (Figure 5D). GalNAc-siChREBP treatment tended to cause a decrease in liver valine ($p = 0.052$) and caused a significant decrease in leucine/iso-leucine ($p = 0.002$) relative to GalNAc-siCtrl treatment (Figure 5A). However, GalNAc-siChREBP treatment had no effect on levels of the branched-chain keto acids ketoisovalerate (KIV), ketoisocaproate (KIC), or ketomethylvalerate (KMV) (Figure 5E). GalNAc-siChREBP treatment also decreased the level of the valine-derived metabolite butyryl/isobutyryl (C4/Ci4) acylcarnitine (Figure 5F). These data, and the absence of any changes in BCKDH or ACLY phosphorylation despite the 75% reduction in BCKDK protein levels, suggest that ChREBP exerts regulatory influences on BCKDH and ACLY beyond the regulation afforded by BCKDK-mediated phosphorylation, a topic that remains to be explored in future studies.

Effects of ChREBP on nucleotide metabolism

Given the multiple unexpected effects of ChREBP suppression on diverse aspects of cellular metabolism, including pathways expected to influence cellular energy homeostasis, we next assessed the effects of ChREBP suppression on nucleotide and purine pathway intermediates using our previously described targeted liquid chromatography-mass spectrometry method.³⁷ We found levels of PRPP, ZMP, and AICAR to be dramatically increased in livers of GalNAc-siChREBP-treated relative to GalNAc-siCtrl-treated rats (Figure 6A; Data S5). PRPP, ZMP, and AICAR are late intermediates in the *de novo* purine biosynthesis pathway, and PRPP is also a co-substrate in the last steps of the *de novo* nicotinamide adenine dinucleotide (NAD) synthesis pathway and purine salvage pathways. In contrast to the increase in these precursors, the products of the purine synthesis pathways inosine monophosphate (IMP), guanosine monophosphate (GMP), and adenosine monophosphate (AMP), as well as products of the *de novo* nicotinamide dinucleotide synthesis pathway, including nicotinic acid mononucleotide (NaMN), NAD(P), and NAD(P)H, were all sharply reduced in livers of GalNAc-siChREBP-treated compared to GalNAc-siCtrl-treated rats (Figures 6A–6C). Interestingly, levels of the nucleotide di-phosphates (adenosine, uridine, guanosine [ADP, UDP, GDP]) or respective nucleotide triphosphates (ATP, UTP, GTP) were not lowered by GalNAc-siChREBP treatment, and UTP was significantly increased (Figure 6D). One possible contributor to the maintenance of nucleotide di- and triphosphate pools is the putative increase in pyruvate oxidation described earlier. We also found levels of phosphocreatine to be significantly increased, while creatine levels exhibited a non-significant trend for a decrease in livers of GalNAc-siChREBP-treated compared to GalNAc-siCtrl-treated rats (Figure S2G). Taken together, these data unveil unanticipated roles of ChREBP in the control of nucleotide metabolism and energy homeostasis.

To further investigate mechanisms underlying these changes, we queried our RNA-seq dataset. The 5-aminoimidazole-4-carboxamide ribonucleotide formyltransferase/inosine monophosphate cyclohydrolase (*Atic*) gene encodes a bifunctional enzyme that includes AICAR transformylase and IMP cyclohydrolase activities to catalyze conversion of AICAR to IMP with N^{10} -formyl tetrahydrofolate as co-substrate for the reaction.

Atic transcript levels were significantly downregulated in livers of GalNAc-siChREBP-treated compared to GalNAc-siCtrl-treated rats by RNA-seq analysis (1.3-fold decrease, $p_{adj} = 0.0001$, Data S3) and trended to decrease when measured by qPCR (Figure 6E). An alternative source of nucleotide monophosphates is the salvage pathway, with hypoxanthine guanine phosphoribosyltransferase (HPRT) serving as a final step in the pathway via its conversion of hypoxanthine to IMP, using PRPP as a co-substrate. *Hprt* transcript levels were sharply decreased in GalNAc-siChREBP-treated compared to GalNAc-siCtrl-treated rats measured both by RNA-seq analysis (1.9-fold decrease, $p_{adj} = 3.7 \times 10^{-32}$) and qPCR (Figure 6E). With regard to the changes in nicotinamide dinucleotide pools, the penultimate enzyme in the *de novo* biosynthesis pathway is quinolinate phosphoribosyltransferase (QPRT), which converts quinolinate derived from the tryptophan/kynurenine metabolism to NaNM and NAD, again using PRPP as a co-substrate. *Qprt* transcript levels were significantly reduced in GalNAc-siChREBP-treated compared to GalNAc-siCtrl-treated rats both in the RNA-seq analysis (1.3-fold reduced, $p_{adj} = 5.5 \times 10^{-11}$) and when measured by qPCR (Figure 6E), consistent with the increased levels of PRPP and lowered levels of NaNM, NAD(H), and NADP(H) in GalNAc-siChREBP-treated rats. Schematic summaries of the impact of ChREBP suppression on purine and NAD synthesis pathways are shown in Figures 6F and 6G, respectively.

We note that calculation of energy change using our values for AMP, ADP, and ATP levels, expressed as $\mu\text{mol/g tissue}$, align with values calculated for livers from 18-h fasted mice³⁸ or mouse liver samples exposed to brief ischemia.³⁹ It is possible in retrospect that some ischemia could have occurred in our study despite our care in executing the tissue dissections (see STAR Methods), given that as little as 30 s of exposure of mouse liver to ischemia lowers energy charge.³⁹ However, we note that ChREBP knockdown had significant and specific effects on levels of a host of intermediates in pathways such as CoA, purine, and nicotinamide dinucleotide metabolism, with increases and decreases in pathway metabolites that aligned perfectly with regulation of transcripts in those same pathways. Also, the surgical procedure was identical for the GalNAc-siChREBP-treated and control groups. Thus, we believe that our results are valid in the context of the experimental methods used.

DISCUSSION

In this study, we have integrated transcriptomic and metabolic analyses to better understand the role of hepatic ChREBP in coordinated regulation of key pathways of intermediary metabolism. Since its discovery in 2001,⁴⁰ ChREBP has emerged as a key regulator of tissue responses to carbohydrate ingestion.^{1,41} It is particularly responsive to fructose, which is consumed in high amounts in modern society via sugar-sweetened beverages and foods containing sucrose or high-fructose corn syrup. Consumption of fructose-containing foods produces carbohydrate metabolites that allosterically activate ChREBP- α , which acts upon an alternative promoter in the ChREBP gene to stimulate transcription of ChREBP- β , the more potent transcriptional

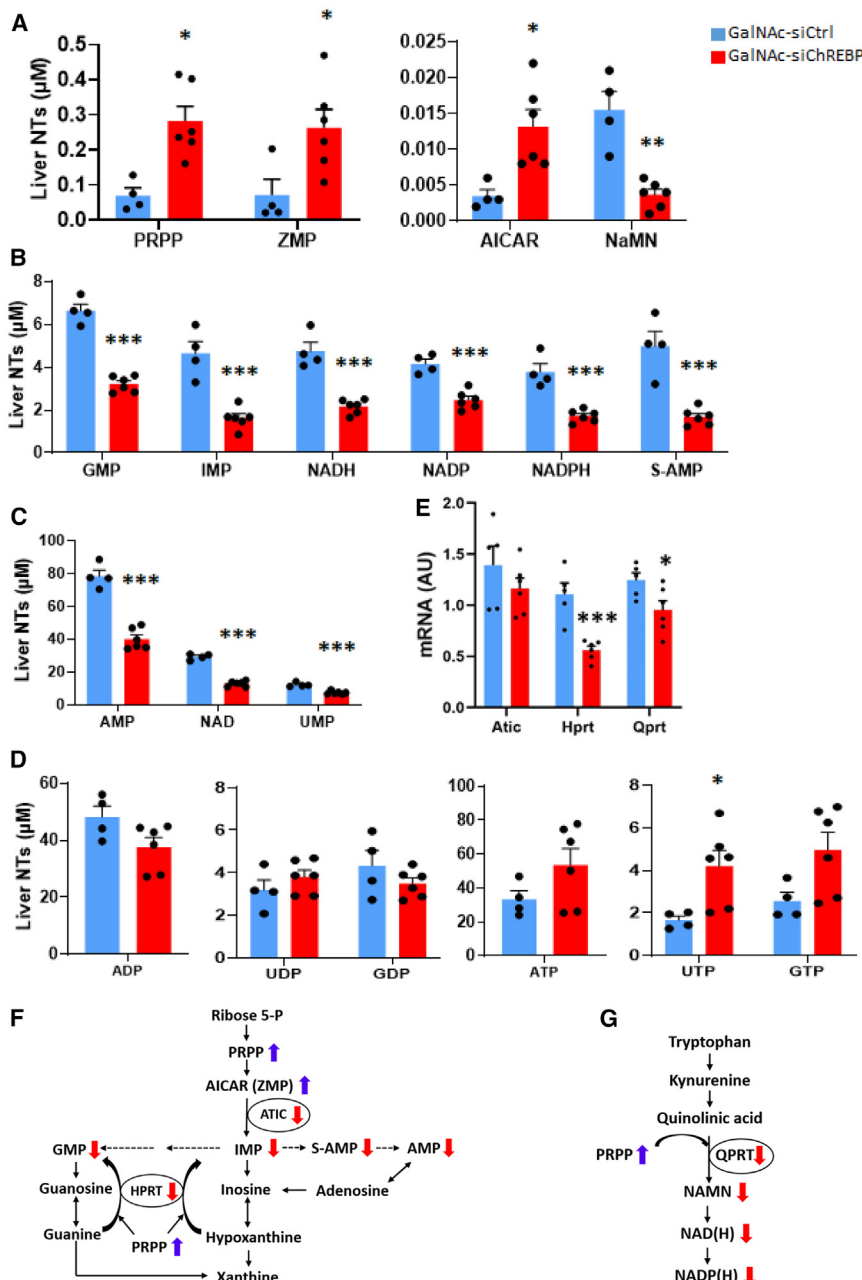


Figure 6. Effects of GalNAc-siChREBP on indices of nucleotide metabolism in liver

(A) Levels of purine and nicotinamide dinucleotide pathway intermediates PRPP, ZMP, AICAR, and NaMN.

(B) Levels of purine and nicotinamide dinucleotide pathway intermediates GMP, IMP, NADH, NADP, NADPH, and S-AMP.

(C) Levels of purine and nicotinamide dinucleotide pathway intermediates AMP, NAD, and UMP.

(D) Levels of nucleotide di- and triphosphate intermediates.

(E) Levels of transcripts involved in pathways of purine or nicotinamide dinucleotide synthesis in liver measured by qPCR, including 5-aminoimidazole-4-carboxamide ribonucleotide formyltransferase/inosine monophosphate cyclohydrolase (Atic), hypoxanthine guanine phosphoribosyltransferase (Hprt), and quinolinate phosphoribosyltransferase (Qprt).

(F) Schematic summary of metabolites and transcripts in purine biosynthesis pathways altered by suppression of ChREBP expression.

(G) Schematic summary of metabolites and transcripts in nicotinamide dinucleotide synthesis pathways altered by suppression of ChREBP expression.

Data are the mean ± SEM for six independent rats/liver samples for the GalNAc-siChREBP-treated group and 4–5 rats/liver samples for the GalNAc-siCtrl group. Statistical analysis performed using unpaired t test or multiple t test. Asterisks indicate differences in the GalNAc-siChREBP treatment group compared to the GalNAc-siCtrl group, with * $p < 0.05$, ** $p < 0.01$, and *** $p < 0.001$. Metabolite levels for individual rat livers are presented in Data S5.

activator among the two ChREBP isoforms.⁴² The transcriptional programs activated by ChREBP- α and ChREBP- β enhance metabolism of carbohydrates to form lipids via the glycolytic and DNL pathways. ChREBP also has homeostatic functions, such as activation of glucose-6-phosphatase expression to limit accumulation of glycogen during periods of increased carbohydrate influx^{3,18,21} and activation of transmembrane 6 superfamily member 2 (*Tm6sf2*) expression¹⁸ to stimulate lipid export in VLDL particles, thereby limiting TG overaccumulation.

Here, we have uncovered functions of ChREBP in regulation of metabolic pathways that are associated with, but distinct from, core pathways of glucose and lipid metabolism. Our approach

to data analysis was to allow ChREBP-mediated metabolite changes to point us to pathways in which to query potential underlying transcriptomic changes. This method identified pathways that were not identified by cluster or pathway analyses of the transcriptomic data, suggesting an alternative metabolite-driven approach to integration of multi-omics datasets. By focusing on transcripts and metabolites specifically altered by

GalNAc-siChREBP versus GalNAc-siCtrl treatment of HF/HS-fed rats, pathways identified as regulated by ChREBP included (1) biosynthesis of free CoA, resulting in decreased levels of free CoA and several short-chain acyl-CoA metabolites, including acetyl-CoA, butyryl-CoA, HMG-CoA, and propionyl-CoA, presumably secondary to the depletion of the free CoA pool; (2) regulation of a broad array of genes involved in pyruvate metabolism, including multiple isoforms of the monocarboxylic acid carrier (SLCa16) gene family, *Ldha*, glutamate/pyruvate transaminase 2 (*Gpt2*), and *Pk1r*, which in aggregate may “funnel” pyruvate for use in PDH-mediated oxidation; (3) reduced purine biosynthesis by *de novo* and salvage pathways, highlighted

by the large increase in the co-substrates PRPP and AICAR and the fall in nucleotide monophosphate levels (AMP, IMP, GMP), aligned with suppression of transcripts encoding the key *de novo* pathway enzyme ATIC and salvage pathway enzyme HPRT (Figure 6F); nicotinamide mononucleotide (NaNM) and nicotinamide adenine nucleotides (NADP(H) and NAD(H)) were also decreased, aligned with lowered expression of the late *de novo* synthesis pathway transcript QPRT, another PRPP utilizing enzyme (Figure 6G); (4) suppression of transcripts encoding multiple anaplerotic enzymes, including *Pc*, *Gdh*, *Got1*, and *Got2*; and (5) lowering of multiple amino acid levels, accompanied by upregulation of a set of transcripts encoding plasma membrane amino acid transporters.

These broad effects of ChREBP on diverse metabolic pathways have been revealed by suppressing expression of the transcription factor in a liver-selective fashion with GalNAc-siRNA technology in rats fed an HF/HS diet. These findings predict the inverse effects of ChREBP under conditions where its activity is induced by carbohydrate feeding. In that context, the predicted concerted induction of genes involved in CoA synthesis likely facilitates conversion of fructose and glucose to CoA-modified intermediates required for mitochondrial energy metabolism and DNL, as well as modification of newly synthesized fatty acids to form fatty acyl-CoAs, a required step for their utilization in both esterification and oxidation reactions. Similarly, ChREBP-mediated activation of glucose and fructose metabolism via well-known targets such as *Slc2a2* (GLUT-2) and *Slc2a5* (GLUT-5), glucokinase regulatory protein, ketohexokinase, and pyruvate kinase must be accompanied by expression of anaplerotic enzymes to fuel increased TCA cycle flux for generation of cataplerotic/lipogenic intermediates, consistent with our finding of robust regulation of four such enzymes—PC, GDH, GOT1, and GOT2. Our study also expands upon and helps explain earlier observations of increased pyruvate utilization in liver of global ChREBP knockout in mice¹³ via our observations of upregulation of multiple monocarboxylic acid carrier family members to facilitate pyruvate uptake, and preservation of the pyruvate pool by suppression of *Ldha* and *Gpt2*. Interestingly, in the earlier study, feeding of mice with global knockout of ChREBP on a HS diet resulted in starvation and death,¹³ suggesting that a switch to high reliance on pyruvate as the major oxidative fuel becomes untenable in the global knockout setting, whereas in our studies of liver-selective ChREBP knockdown, body weight and survival were maintained even with feeding of an HF/HS diet. Finally, our findings suggest that ChREBP-mediated disposal of glucose and fructose requires coordinated upregulation of nucleotide and nicotinamide dinucleotide synthesis to support energy and redox-requiring pathways, including glycogen synthesis, DNL, acylation of fatty acids, and lipid esterification and packaging.

Our finding of an effect of ChREBP suppression to increase expression of a set of plasma membrane amino acid carriers is consistent with a model in which suppression of ChREBP activates amino acid catabolism at a time when anaplerotic substrate influx from glucose or other sugars is limited due to impaired glycolysis. Conversely, when ChREBP is activated by carbohydrate feeding, this may serve to suppress expression of amino acid transporters to help limit gluconeogenesis from amino acids at a time when glucose is readily available.

Knockdown of ChREBP expression in liver of HF/HS-fed rats had complex effects on lipid metabolism. Some, but not all, of these effects were previously reported in studies involving partial ChREBP knockdown in a mouse model of glycogen storage disease type 1 or ASO-mediated knockdown of ChREBP in fructose-fed rats, or in other models.^{4,10,17,18} In the current study, while knockdown of ChREBP in the liver decreased DNL, it also increased total hepatic fatty acid and TG content. In addition, while increasing lipid storage in liver, knockdown of ChREBP affected indices suggestive of increased FAO, including an increase in transcripts encoding the four core enzymes of mitochondrial FAO, reduced circulating NEFA, increased circulating ketone levels, and increases in a wide array of fatty-acid-derived acylcarnitine species in liver. Our findings suggest that hepatic ChREBP knockdown results in an activation of FAO to the level of acetyl-CoA, some of which is diverted to ketones, but the bulk of which fails to be fully oxidized due to limitations in supply of free CoA, NAD(P), and anaplerotic substrates. When viewed in this light, the accumulation of a broad spectrum of liver acylcarnitines may reflect a bottleneck in complete oxidation of fatty acids, as has also been described in skeletal muscle in obesity.²⁹ Mice with global ChREBP knockout have been reported to have reduced rates of complete FAO in perfused livers relative to wild-type mice, measured indirectly by dilution of [¹³C]glutamate labeling, seemingly consistent with our findings, but in the prior study accompanied by a significant decrease in ketone production,¹³ unlike what we observed. This apparent discrepancy may have been related to their use of global ChREBP knockout mice in which metabolic effects of ChREBP loss would be manifest in extrahepatic tissues, as opposed to our strategy of targeted suppression of ChREBP in liver of rats fed on HF/HS diet.

Overall, our lipid metabolism-related data provide new support for the concept that ChREBP is a transcription factor that seeks metabolic equilibrium when the system is challenged by carbohydrate feeding. When viewed in this way, increases in hepatic fatty acid and TG content observed here in response to ChREBP suppression are counterbalanced by a decrease in DNL and an increase in FAO. The observed increases in hepatic TG and fatty acids under these conditions may be driven by the decrease in *Tm6sf2* expression and increased *Cd36* expression, allowing the liver to preserve lipid stores during a period of reduced fatty acid synthesis and increased FAO. Our transcriptomic analysis suggests involvement of other regulatory genes in mediating this complex response to ChREBP suppression, including the decrease in expression of *Rgs16* and the decrease in expression of key genes in the DNL pathway, *Pklr*, *Acy1*, *Acaca*, and *Fasn*. The converse of our findings with ChREBP suppression is that activation by carbohydrate feeding would result in an increase in DNL, a decrease in FAO, and an increase in lipid storage, but modulated by increased lipid export from the liver as VLDL and a decrease in fatty acid uptake. We note that in humans, a common missense variant of ChREBP (*MLXIPL*, *Gln241His*) is associated with strong lowering of circulating TG and an increase in steatotic liver disease,⁴³ suggestive of increased hepatic TG storage. These phenotypes seem to align with our findings (Figures 1G and 1H).

Our interest in further investigation of metabolic regulatory effects of ChREBP in liver was stimulated in part by our recent

finding that the BCKDH kinase (BCKDK) and phosphatase (PPM1K) are regulated by ChREBP and that ACLY is an alternative BCKDK and PPM1K substrate.¹² Thus, adenovirus-mediated ChREBP- β expression in liver recapitulates the effects of fructose feeding on *Bckdk* and *Ppm1k* expression¹² and is sufficient to increase phosphorylation of ACLY and *de novo* lipogenesis.¹² This mechanism may contribute to the association of BCAAs with type 2 diabetes⁴⁴ as well as an association of branched-chain ketoacids (BCKAs) and BCKDK with nonalcoholic fatty liver disease/nonalcoholic steatohepatitis that we have recently described in human subjects.⁴⁵ In the current study, treatment of rats with GalNAc-siChREBP caused a significant decrease in *Bckdk* mRNA and protein levels, consistent with the increase in expression of *Bckdk* in liver observed with ChREBP- β overexpression.¹² Here, we also found that ChREBP knockdown caused an increase in expression of the E2 component (lipoamide acyltransferase, *Dbt*) of the BCKDH complex as well as isovaleryl-CoA dehydrogenase (*Ivd*), the third enzyme in catabolism of leucine, providing further evidence for a role of ChREBP in regulation of BCAAs and amino acid metabolism. However, whereas GalNAc-siChREBP treatment resulted in a 75% decrease in BCKDK protein levels, this had no effect on BCKDH phosphorylation. Moreover, while GalNAc-siChREBP treatment reduced phospho-ACLY levels, this effect could be explained by a decrease in total ACLY protein.

These findings suggest that additional factors may be involved in mediating interactions between ChREBP, BCKDK, ACLY, and BCKDH. Our findings may have been influenced by the multiple new metabolic effects of ChREBP suppression uncovered in this study. Also, the prior studies were performed in lean male Wistar rats or in male Zucker-obese and Zucker-lean rats fed on standard chow diet, while the current study involved obesity-prone (OP-CD) male Sprague-Dawley rats fed an HF/HS diet, suggesting that nutritional status or genetics could have contributed to the discordant findings. Other recent work by our group suggests that careful attention must be paid to species (e.g., mouse versus rat versus human)^{12,46} and sex in analysis of this regulatory node. For example, rats, non-human primates, and humans all contain a ChREBP binding sequence in the promoter region of their BCKDK genes, whereas mice lack this motif.¹²

Limitations of the study

A limitation of the study is in discerning direct versus indirect effects of ChREBP in mediating the metabolic changes reported here. Some insight can be gained from a prior ChIP-sequencing study from our group performed in the mouse.⁴⁷ Among genes implicated as ChREBP regulated in the current study, those encoding the anaplerotic enzyme *Got2*, the short-chain acyl-CoA metabolizing enzyme *Crat*, the PDH kinase *Pdk4*, the E2 component of the PDH complex *Pdhb*, and lactate dehydrogenase *Ldha* all contain ChIP-sequencing peaks indicative of ChREBP binding in the mouse genome. However, genes identified as downregulated by suppression of ChREBP in other pathways such as purine/NAD(P) synthesis, CoA synthesis, and amino acid transport do not have obvious ChREBP-regulatory elements in the mouse genome. This may indicate an intrinsic difference in ChREBP regulation of genes in the rat versus the mouse, as shown for BCKDK, or possibly indirect regulatory mechanisms,

for example involving ChREBP-mediated changes in metabolites or proteins that influence functions of other transcription factors or co-regulators in the rat. Gaining full understanding of these mechanisms is an ultimate future goal of our work. We also note the need to expand our studies to include analysis of the effects of manipulation of ChREBP in male versus female rats, under different nutritional conditions, and in different genetic backgrounds.

In sum, by combining metabolomic and transcriptomic analyses, we have uncovered regulatory effects of ChREBP on metabolic homeostasis beyond its historical role in control of core glucose and lipid metabolic pathways to now include effects on co-factors, transporters for amino acids and other small molecules, nucleotide metabolism, and control of mitochondrial substrate supply.

RESOURCE AVAILABILITY

Lead contact

Requests for further information, resources, and reagents should be directed to and will be fulfilled by the lead contact, Christopher B. Newgard, PhD (chris.newgard@duke.edu).

Materials availability

The GalNAc-siRNA constructs used in this study were prepared by Biosynthesis, Inc., Lewisville, TX using a protocol described in the [STAR Methods](#), and interested parties should inquire with the company to obtain this material. No other unique reagents were generated in this study.

Data and code availability

- With regard to data, targeted metabolomics and conventional analyte data for individual animals can be found in [Data S5](#), and raw data have been deposited at Metabolomics Workbench, with the accession number shown in the [key resources table](#) and the [STAR Methods](#). RNA-seq data can be found in [Data S1](#), [S2](#), [S3](#), and [S4](#) and have been deposited in the GEO database, with accession numbers shown in the [key resources table](#) and the [STAR Methods](#).
- Code used for processing RNA-seq data is provided in the [STAR Methods](#) in the [RNA sequencing and analysis](#) section.
- Regarding all other items, no new or novel code was generated for data analyses reported here. Data points for individual animals for physiological measures such as body weight, glucose levels during glucose tolerance testing, liver glycogen, liver weight, and measurements of *de novo* lipogenesis are shown in the respective figures, and the raw data for such measurements can be provided on request.

ACKNOWLEDGMENTS

The authors are grateful to Ms. Helena Winfield for expert technical assistance in the animal studies. This work was supported by National Institutes of Health grants DK12170 (to C.B.N. and M.A.H.), DK124723 (to C.B.N.), and DK100425 (to M.A.H.). The NIH Metabolomics Workbench is supported by NIH grants U2C-DK119886 and OT2-OD030544. We thank Dr. Anish Konkar and Eli Lilly for their gift of GalNAc-siRNA reagents used in this study.

AUTHOR CONTRIBUTIONS

Conceptualization, J.A., I.A., M.A.H., and C.B.N.; methodology, J.A., I.A., J.B., M.A.H., and C.B.N.; validation, J.A., I.A., M.A.H., and C.B.N.; formal analysis, J.A., I.A., M.A.H., and C.B.N.; investigation, J.A., I.A., G.Z., A.L.C., O.I., H.M., M.J.M., and T.G.; writing – original draft, C.B.N.; writing – review & editing, J.A., I.A., G.Z., M.A.H., and C.B.N.; visualization, J.A., I.A., A.L.C., and M.A.H.; supervision, M.A.H. and C.B.N.; project administration, M.A.H. and C.B.N.; funding acquisition, M.A.H. and C.B.N.

DECLARATION OF INTERESTS

C.B.N. is a member of the Global Diabetes Advisory Board at Eli Lilly. All experiments described in this paper were supported by the above-referenced NIH grants. Eli Lilly supplied the GalNAc-siRNA reagents for the studies under a materials transfer agreement at their cost, with no restrictions on publication of data. J.B. is a Lilly employee who collaborated on the project by providing guidance in the use of the GalNAc-siRNA reagents and assistance with interpretation of data generated in their use.

STAR★METHODS

Detailed methods are provided in the online version of this paper and include the following:

- **KEY RESOURCES TABLE**
- **EXPERIMENTAL MODEL AND STUDY PARTICIPANT DETAILS**
 - Administration of GalNAc-siRNA reagents and testing during survival period
 - Tissue harvesting procedure
 - Approval of animal studies
- **METHOD DETAILS**
 - Measurement of hepatic triglycerides and glycogen
 - Construction of GalNAc-siRNAs
 - Metabolomic analyses
 - Conventional metabolites and hormones
 - Measurement of hepatic *de novo* lipogenesis
 - Immunoblotting
 - RNA isolation and qPCR analysis
 - RNA sequencing and analysis
- **QUANTIFICATION AND STATISTICAL ANALYSIS**

SUPPLEMENTAL INFORMATION

Supplemental information can be found online at <https://doi.org/10.1016/j.celrep.2025.115278>.

Received: September 24, 2024

Revised: December 3, 2024

Accepted: January 16, 2025

Published: February 7, 2025

REFERENCES

1. Katz, L.S., Baumel-Alterzon, S., Scott, D.K., and Herman, M.A. (2021). Adaptive and maladaptive roles for ChREBP in the liver and pancreatic islets. *J. Biol. Chem.* 296, 100623. <https://doi.org/10.1016/j.jbc.2021.100623>.
2. Herman, M.A., and Birnbaum, M.J. (2021). Molecular aspects of fructose metabolism and metabolic disease. *Cell Metabol.* 33, 2329–2354. <https://doi.org/10.1016/j.cmet.2021.09.010>.
3. Kim, M.-S., Krawczyk, S.A., Doridot, L., Fowler, A.J., Wang, J.X., Trauger, S.A., Noh, H.-L., Kang, H.J., Meissen, J.K., Blatnik, M., et al. (2016). ChREBP regulates fructose-induced glucose production independently of insulin signaling. *J. Clin. Invest.* 126, 4372–4386. <https://doi.org/10.1172/JCI181993>.
4. Kim, M., Astapova, I.I., Flier, S.N., Hannou, S.A., Doridot, L., Sargsyan, A., Kou, H.H., Fowler, A.J., Liang, G., and Herman, M.A. (2017). Intestinal, but not hepatic, ChREBP is required for fructose tolerance. *JCI Insight* 2, e96703. <https://doi.org/10.1172/jci.insight.96703>.
5. Doridot, L., Hannou, S.A., Krawczyk, S.A., Tong, W., Kim, M.-S., McElroy, G.S., Fowler, A.J., Astapova, I.I., and Herman, M.A. (2021). A Systems Approach Dissociates Fructose-Induced Liver Triglyceride from Hypertriglyceridemia and Hyperinsulinemia in Male Mice. *Nutrients* 13, 3642. <https://doi.org/10.3390/nu13103642>.
6. Kawaguchi, T., Takenoshita, M., Kabashima, T., and Uyeda, K. (2001). Glucose and cAMP regulate the L-type pyruvate kinase gene by phosphorylation/dephosphorylation of the carbohydrate response element binding protein. *Proc. Natl. Acad. Sci. USA* 98, 13710–13715. <https://doi.org/10.1073/pnas.231370798>.
7. Iizuka, K., Bruick, R.K., Liang, G., Horton, J.D., and Uyeda, K. (2004). Deficiency of carbohydrate response element-binding protein (ChREBP) reduces lipogenesis as well as glycolysis. *Proc. Natl. Acad. Sci. USA* 101, 7281–7286. <https://doi.org/10.1073/pnas.0401516101>.
8. Dentin, R., Benhamed, F., Hainault, I., Fauveau, V., Foufelle, F., Dyck, J.R.B., Girard, J., and Postic, C. (2006). Liver-specific inhibition of ChREBP improves hepatic steatosis and insulin resistance in ob/ob mice. *Diabetes* 55, 2159–2170. <https://doi.org/10.2337/db06-0200>.
9. Iizuka, K., Miller, B., and Uyeda, K. (2006). Deficiency of carbohydrate-activated transcription factor ChREBP prevents obesity and improves plasma glucose control in leptin-deficient (ob/ob) mice. *Am. J. Physiol. Endocrinol. Metab.* 291, E358–E364. <https://doi.org/10.1152/ajpendo.00027.2006>.
10. Erion, D.M., Popov, V., Hsiao, J.J., Vatner, D., Mitchell, K., Yonemitsu, S., Nagai, Y., Kahn, M., Gillum, M.P., Dong, J., et al. (2013). The role of the carbohydrate response element-binding protein in male fructose-fed rats. *Endocrinology* 154, 36–44. <https://doi.org/10.1210/en.2012-1725>.
11. Ma, L., Robinson, L.N., and Towle, H.C. (2006). ChREBP*Mix is the principal mediator of glucose-induced gene expression in the liver. *J. Biol. Chem.* 281, 28721–28730. <https://doi.org/10.1074/jbc.M601576200>.
12. White, P.J., McGarrah, R.W., Grimsrud, P.A., Tso, S.-C., Yang, W.-H., Haldeman, J.M., Grenier-Larouche, T., An, J., Lapworth, A.L., Astapova, I., et al. (2018). The BCKDH Kinase and Phosphatase Integrate BCAA and Lipid Metabolism via Regulation of ATP-Citrate Lyase. *Cell Metabol.* 27, 1281–1293.e7. <https://doi.org/10.1016/j.cmet.2018.04.015>.
13. Burgess, S.C., Iizuka, K., Jeoung, N.H., Harris, R.A., Kashiwaya, Y., Veech, R.L., Kitazume, T., and Uyeda, K. (2008). Carbohydrate-response element-binding protein deletion alters substrate utilization producing an energy-deficient liver. *J. Biol. Chem.* 283, 1670–1678. <https://doi.org/10.1074/jbc.M706540200>.
14. Wang, Y., Yu, R.Z., Henry, S., and Geary, R.S. (2019). Pharmacokinetics and Clinical Pharmacology Considerations of GalNAc3-Conjugated Antisense Oligonucleotides. *Expert Opin. Drug Metabol. Toxicol.* 15, 475–485. <https://doi.org/10.1080/17425255.2019.1621838>.
15. Singh, C., Jin, B., Shrestha, N., Markhard, A.L., Panda, A., Calvo, S.E., Deik, A., Pan, X., Zuckerman, A.L., Ben Saad, A., et al. (2024). ChREBP is activated by reductive stress and mediates GCKR-associated metabolic traits. *Cell Metabol.* 36, 144–158.e7. <https://doi.org/10.1016/j.cmet.2023.11.010>.
16. Yenilmez, B., Kelly, M., Zhang, G.-F., Wetoska, N., Ilkayeva, O.R., Min, K., Rowland, L., DiMarzio, C., He, W., Raymond, N., et al. (2022). Paradoxical activation of transcription factor SREBP1c and *de novo* lipogenesis by hepatocyte-selective ATP-citrate lyase depletion in obese mice. *J. Biol. Chem.* 298, 102401. <https://doi.org/10.1016/j.jbc.2022.102401>.
17. Linden, A.G., Li, S., Choi, H.Y., Fang, F., Fukasawa, M., Uyeda, K., Hammer, R.E., Horton, J.D., Engelking, L.J., and Liang, G. (2018). Interplay between ChREBP and SREBP-1c coordinates postprandial glycolysis and lipogenesis in livers of mice. *J. Lipid Res.* 59, 475–487. <https://doi.org/10.1194/jlr.M081836>.
18. Lei, Y., Hoogerland, J.A., Bloks, V.W., Bos, T., Bleeker, A., Wolters, H., Wolters, J.C., Hijmans, B.S., van Dijk, T.H., Thomas, R., et al. (2020). Hepatic Carbohydrate Response Element Binding Protein Activation Limits Nonalcoholic Fatty Liver Disease Development in a Mouse Model for Glycogen Storage Disease Type 1a. *Hepatology* 72, 1638–1653. <https://doi.org/10.1002/hep.31198>.
19. Niwa, H., Iizuka, K., Kato, T., Wu, W., Tsuchida, H., Takao, K., Horikawa, Y., and Takeda, J. (2018). ChREBP Rather Than SHP Regulates Hepatic VLDL Secretion. *Nutrients* 10, 321. <https://doi.org/10.3390/nu10030321>.

20. Smagris, E., Gilyard, S., BasuRay, S., Cohen, J.C., and Hobbs, H.H. (2016). Inactivation of Tm6sf2, a Gene Defective in Fatty Liver Disease, Impairs Lipidation but Not Secretion of Very Low Density Lipoproteins. *J. Biol. Chem.* 291, 10659–10676. <https://doi.org/10.1074/jbc.M116.719955>.
21. Shi, J.-H., Lu, J.-Y., Chen, H.-Y., Wei, C.-C., Xu, X., Li, H., Bai, Q., Xia, F.-Z., Lam, S.M., Zhang, H., et al. (2020). Liver ChREBP Protects Against Fructose-Induced Glycogenic Hepatotoxicity by Regulating L-Type Pyruvate Kinase. *Diabetes* 69, 591–602. <https://doi.org/10.2337/db19-0388>.
22. Dong, B., Saha, P.K., Huang, W., Chen, W., Abu-Elheiga, L.A., Wakil, S.J., Stevens, R.D., Ilkayeva, O., Newgard, C.B., Chan, L., and Moore, D.D. (2009). Activation of nuclear receptor CAR ameliorates diabetes and fatty liver disease. *Proc. Natl. Acad. Sci. USA* 106, 18831–18836. <https://doi.org/10.1073/pnas.0909731106>.
23. Fisher, F.M., Kim, M., Doridot, L., Cunniff, J.C., Parker, T.S., Levine, D.M., Hellerstein, M.K., Hudgins, L.C., Maratos-Flier, E., and Herman, M.A. (2017). A critical role for ChREBP-mediated FGF21 secretion in hepatic fructose metabolism. *Mol. Metabol.* 6, 14–21. <https://doi.org/10.1016/j.molmet.2016.11.008>.
24. Dowdy, S.F. (2017). Overcoming cellular barriers for RNA therapeutics. *Nat. Biotechnol.* 35, 222–229. <https://doi.org/10.1038/nbt.3802>.
25. McGarrah, R.W., Zhang, G.-F., Christopher, B.A., Deleye, Y., Walejko, J.M., Page, S., Ilkayeva, O., White, P.J., and Newgard, C.B. (2020). Dietary branched-chain amino acid restriction alters fuel selection and reduces tri-glyceride stores in hearts of Zucker fatty rats. *Am. J. Physiol. Endocrinol. Metab.* 318, E216–E223. <https://doi.org/10.1152/ajpendo.00334.2019>.
26. An, J., Muoio, D.M., Shiota, M., Fujimoto, Y., Cline, G.W., Shulman, G.I., Koves, T.R., Stevens, R., Millington, D., and Newgard, C.B. (2004). Hepatic expression of malonyl-CoA decarboxylase reverses muscle, liver and whole-animal insulin resistance. *Nat. Med.* 10, 268–274. <https://doi.org/10.1038/nm995>.
27. Herman, M.A., She, P., Peroni, O.D., Lynch, C.J., and Kahn, B.B. (2010). Adipose tissue branched chain amino acid (BCAA) metabolism modulates circulating BCAA levels. *J. Biol. Chem.* 285, 11348–11356. <https://doi.org/10.1074/jbc.M109.075184>.
28. Pashkov, V., Huang, J., Parameswara, V.K., Kedzierski, W., Kurrasch, D.M., Tall, G.G., Esser, V., Gerard, R.D., Uyeda, K., Towle, H.C., and Wilkie, T.M. (2011). Regulator of G protein signaling (RGS16) inhibits hepatic fatty acid oxidation in a carbohydrate response element-binding protein (ChREBP)-dependent manner. *J. Biol. Chem.* 286, 15116–15125. <https://doi.org/10.1074/jbc.M110.216234>.
29. Koves, T.R., Ussher, J.R., Noland, R.C., Slentz, D., Mosedale, M., Ilkayeva, O., Bain, J., Stevens, R., Dyck, J.R.B., Newgard, C.B., et al. (2008). Mitochondrial overload and incomplete fatty acid oxidation contribute to skeletal muscle insulin resistance. *Cell Metabol.* 7, 45–56. <https://doi.org/10.1016/j.cmet.2007.10.013>.
30. White, P.J., Lapworth, A.L., An, J., Wang, L., McGarrah, R.W., Stevens, R.D., Ilkayeva, O., George, T., Muehlbauer, M.J., Bain, J.R., et al. (2016). Branched-chain amino acid restriction in Zucker-fatty rats improves muscle insulin sensitivity by enhancing efficiency of fatty acid oxidation and acyl-glycine export. *Mol. Metabol.* 5, 538–551. <https://doi.org/10.1016/j.molmet.2016.04.006>.
31. Ferrara, C.T., Wang, P., Neto, E.C., Stevens, R.D., Bain, J.R., Wenner, B.R., Ilkayeva, O.R., Keller, M.P., Blasiole, D.A., Kendziora, C., et al. (2008). Genetic networks of liver metabolism revealed by integration of metabolic and transcriptional profiling. *PLoS Genet.* 4, e1000034. <https://doi.org/10.1371/journal.pgen.1000034>.
32. Zamboni, N., Maaheimo, H., Szyperski, T., Hohmann, H.-P., and Sauer, U. (2004). The phosphoenolpyruvate carboxykinase also catalyzes C3 carboxylation at the interface of glycolysis and the TCA cycle of *Bacillus subtilis*. *Metab. Eng.* 6, 277–284. <https://doi.org/10.1016/j.ymben.2004.03.001>.
33. Modaressi, S., Brechtel, K., Christ, B., and Jungermann, K. (1998). Human mitochondrial phosphoenolpyruvate carboxykinase 2 gene. Structure, chromosomal localization and tissue-specific expression. *Biochem. J.* 333, 359–366. <https://doi.org/10.1042/bj3330359>.
34. Méndez-Lucas, A., Duarte, J.A.G., Sunny, N.E., Satapati, S., He, T., Fu, X., Bermúdez, J., Burgess, S.C., and Perales, J.C. (2013). PEPCK-M expression in mouse liver potentiates, not replaces, PEPCK-C mediated gluconeogenesis. *J. Hepatol.* 59, 105–113. <https://doi.org/10.1016/j.jhep.2013.02.020>.
35. Velázquez-Villegas, L., Noriega, L.G., López-Barradas, A.M., Tobon-Cornejo, S., Méndez-García, A.L., Tovar, A.R., Torres, N., and Ortiz-Ortega, V.M. (2021). ChREBP downregulates SNAT2 amino acid transporter expression through interactions with SMRT in response to a high-carbohydrate diet. *Am. J. Physiol. Endocrinol. Metab.* 320, E102–E112. <https://doi.org/10.1152/ajpendo.00326.2020>.
36. Go, Y., Jeong, J.Y., Jeoung, N.H., Jeon, J.-H., Park, B.-Y., Kang, H.-J., Ha, C.-M., Choi, Y.-K., Lee, S.J., Ham, H.J., et al. (2016). Inhibition of Pyruvate Dehydrogenase Kinase 2 Protects Against Hepatic Steatosis Through Modulation of Tricarboxylic Acid Cycle Anaplerosis and Ketogenesis. *Diabetes* 65, 2876–2887. <https://doi.org/10.2337/db16-0223>.
37. Gooding, J.R., Jensen, M.V., Dai, X., Wenner, B.R., Lu, D., Arumugam, R., Ferdaoussi, M., MacDonald, P.E., and Newgard, C.B. (2015). Adenylosuccinate Is an Insulin Secretagogue Derived from Glucose-Induced Purine Metabolism. *Cell Rep.* 13, 157–167. <https://doi.org/10.1016/j.celrep.2015.08.072>.
38. Berglund, E.D., Lee-Young, R.S., Lustig, D.G., Lynes, S.E., Donahue, E.P., Camacho, R.C., Meredith, M.E., Magnuson, M.A., Charron, M.J., and Wasserman, D.H. (2009). Hepatic energy state is regulated by glucagon receptor signaling in mice. *J. Clin. Invest.* 119, 2412–2422. <https://doi.org/10.1172/jci38650>.
39. Fu, X., Deja, S., Kucejova, B., Duarte, J.A.G., McDonald, J.G., and Burgess, S.C. (2019). Targeted Determination of Tissue Energy Status by LC-MS/MS. *Anal. Chem.* 91, 5881–5887. <https://doi.org/10.1021/acs.analchem.9b00217>.
40. Yamashita, H., Takenoshita, M., Sakurai, M., Bruick, R.K., Henzel, W.J., Shillinglaw, W., Arnot, D., and Uyeda, K. (2001). A glucose-responsive transcription factor that regulates carbohydrate metabolism in the liver. *Proc. Natl. Acad. Sci. USA* 98, 9116–9121. <https://doi.org/10.1073/pnas.161284298>.
41. Régnier, M., Carbinatti, T., Parlati, L., Benhamed, F., and Postic, C. (2023). The role of ChREBP in carbohydrate sensing and NAFLD development. *Nat. Rev. Endocrinol.* 19, 336–349. <https://doi.org/10.1038/s41574-023-0089-4>.
42. Herman, M.A., Peroni, O.D., Villoria, J., Schön, M.R., Abumrad, N.A., Blüher, M., Klein, S., and Kahn, B.B. (2012). A novel ChREBP isoform in adipose tissue regulates systemic glucose metabolism. *Nature* 484, 333–338. <https://doi.org/10.1038/nature10986>.
43. Hehl, L., Creasy, K.T., Vitali, C., Scorletti, E., Seeling, K.S., Vell, M.S., Rendel, M.D., Conlon, D., Vujkovic, M., Zandvakili, I., et al. (2024). A genome-first approach to variants in MLXIPL and their association with hepatic steatosis and plasma lipids. *Hepatol. Commun.* 8, e0427. <https://doi.org/10.1097/HC9.0000000000000427>.
44. White, P.J., McGarrah, R.W., Herman, M.A., Bain, J.R., Shah, S.H., and Newgard, C.B. (2021). Insulin action, type 2 diabetes, and branched-chain amino acids: A two-way street. *Mol. Metabol.* 52, 101261. <https://doi.org/10.1016/j.molmet.2021.101261>.
45. Grenier-Larouche, T., Coulter Kwee, L., Deleye, Y., Leon-Mimila, P., Walejko, J.M., McGarrah, R.W., Marceau, S., Trahan, S., Racine, C., Carpenter, A.C., et al. (2022). Altered branched-chain α -ketoo acid metabolism is a feature of NAFLD in individuals with severe obesity. *JCI Insight* 7, e159204. <https://doi.org/10.1172/jci.insight.159204>.
46. Lee, J., Vijayakumar, A., White, P.J., Xu, Y., Ilkayeva, O., Lynch, C.J., Newgard, C.B., and Kahn, B.B. (2021). BCAA Supplementation in Mice with Diet-induced Obesity Alters the Metabolome Without Impairing Glucose Homeostasis. *Endocrinology* 162, bqab062. <https://doi.org/10.1210/en-docr/bqab062>.

47. Sargsyan, A., Doridot, L., Hannou, S.A., Tong, W., Srinivasan, H., Ivison, R., Monn, R., Kou, H.H., Haldeman, J.M., Arlotto, M., et al. (2023). HGFAC is a ChREBP-regulated hepatokine that enhances glucose and lipid homeostasis. *JCI Insight* 8, e153740. <https://doi.org/10.1172/jci.insight.153740>.
48. Bray, N.L., Pimentel, H., Melsted, P., and Pachter, L. (2016). Near-optimal probabilistic RNA-seq quantification. *Nat. Biotechnol.* 34, 525–527. <https://doi.org/10.1038/nbt.3519>.
49. Love, M.I., Huber, W., and Anders, S. (2014). Moderated estimation of fold change and dispersion for RNA-seq data with DESeq2. *Genome Biol.* 15, 550. <https://doi.org/10.1186/s13059-014-0550-8>.
50. Kuleshov, M.V., Jones, M.R., Rouillard, A.D., Fernandez, N.F., Duan, Q., Wang, Z., Koplev, S., Jenkins, S.L., Jagodnik, K.M., Lachmann, A., et al. (2016). Enrichr: a comprehensive gene set enrichment analysis web server 2016 update. *Nucleic Acids Res.* 44, W90–W97. <https://doi.org/10.1093/nar/gkw377>.
51. Monetti, M., Levin, M.C., Watt, M.J., Sajan, M.P., Marmor, S., Hubbard, B.K., Stevens, R.D., Bain, J.R., Newgard, C.B., Farese, R.V., et al. (2007). Dissociation of hepatic steatosis and insulin resistance in mice overexpressing DGAT in the liver. *Cell Metabol.* 6, 69–78. <https://doi.org/10.1016/j.cmet.2007.05.005>.
52. Datta, S., Antonio, B.M., Zahler, N.H., Theile, J.W., Krafte, D., Zhang, H., Rosenberg, P.B., Chaves, A.B., Muoio, D.M., Zhang, G., et al. (2024). APOL1-mediated monovalent cation transport contributes to APOL1-mediated podocytopathy in kidney disease. *J. Clin. Invest.* 134, e172262. <https://doi.org/10.1172/JCI172262>.
53. Sud, M., Fahy, E., Cotter, D., Azam, K., Vadivelu, I., Burant, C., Edison, A., Fiehn, O., Higashi, R., Nair, K.S., et al. (2016). Metabolomics Workbench: an international repository for metabolomics data and metadata, metabolite standards, protocols, tutorials and training, and analysis tools. *Nucleic Acids Res.* 44, D463–D470. <https://doi.org/10.21228/M8WC2H>.
54. Tomcik, K., Ibarra, R.A., Sadhukhan, S., Han, Y., Tochtrop, G.P., and Zhang, G.-F. (2011). Isotopomer enrichment assay for very short chain fatty acids and its metabolic applications. *Anal. Biochem.* 410, 110–117. <https://doi.org/10.1016/j.ab.2010.11.030>.

STAR★METHODS

KEY RESOURCES TABLE

REAGENT or RESOURCE	SOURCE	IDENTIFIER
Antibodies		
Phospho-S293-BCKDHA	Abcam	ab200577; RRID:AB_2687944
BCKDH-E1 α	Cell Signaling Technology	90198; RRID: AB_2800155
Phospho-S454/455-ACLY	Cell Signaling Technology	4331; RRID: AB_2257987
ACLY	Cell Signaling Technology	4332; RRID: AB_2223744
BCKDK	Abcam	ab128935; RRID: AB_11142023
Vinculin	Cell Signaling Technology	4650; RRID: AB_10559207
ChREBP	Novus Biologicals	NB400-135; RRID: AB_10002435
TM6SF2	Smagris et al., ²⁰ gift from Dr. H. Hobbs	pAb-505E
IRDye 800CW Donkey Anti-Rabbit IgG	LI-COR Biotech	926-32213; RRID: AB_621848
IRDye 680RD Goat Anti-Mouse IgG	LI-COR Biotech	926-68070; RRID: AB_10956588
Chemicals, peptides, and recombinant proteins		
Deuterium oxide	Sigma-Aldrich	Cat#151882
[2H31]palmitic acid	Sigma-Aldrich	Cat#366897
N-tert-Butyldimethylsilyl-N-methyltrifluoroacetamide	CovaChem	Cat#12107T
Acetonitrile	Fisher Scientific	Cat#22927
Acetone	Fisher Scientific	Cat#A949-4
Chloroform	Sigma-Aldrich	Cat#CX1058
Hydrochloric acid (6M)	Sigma-Aldrich	Cat#84429
Methanol	Fisher Scientific	Cat#A454-4
Perchloric Acid	Sigma-Aldrich	Cat#311421
Formic Acid	Sigma-Aldrich	Cat#695076
Critical commercial assays		
Triglyceride Liquicolor (MONO)	Stanbio	REF#2200-430
Glucose Liquicolor	Stanbio	REF#1070-125
Sterile saline	Covetrus	Reorder#069169
45% Glucose solution, sterile-filtered	MilliporeSigma	Cat#G8769
Nembutal	OAK Pharmaceuticals, Inc.	NDC 76478-501-50
TRI Reagent	MilliporeSigma	Cat#T9424
SuperScript VILO Master Mix	Thermo Fisher Scientific	Cat#11755500
PowerUp SYBR Green Master Mix for qPCR	Thermo Fisher Scientific	Cat#A25778
Glucose	Beckman	Ref#B24985
Triglyceride and glycerol	Beckman	Ref#445850
NEFA-HR(2) Color A	Fujifilm	#999-34691
NEFA-HR(2) Solvent A	Fujifilm	#995-34791
NEFA-HR(2) Color B	Fujifilm	#991-34891
NEFA-HR(2) Solvent B	Fujifilm	#993-35191
3-HB R1	Fujifilm	#417-73501
3-HB R2	Fujifilm	#413-73601
KET R1	Fujifilm	#415-73301
KET R2	Fujifilm	#411-73401
Rat/Mouse insulin	Meso Scale Discovery	Cat#K152BZC-1

(Continued on next page)

Continued

REAGENT or RESOURCE	SOURCE	IDENTIFIER
Deposited data		
Rat liver RNA sequencing data	This paper	GEO: GSE282614
Rat reference genome assembly mRatBN7.2	Wellcome Sanger Institute	https://www.ncbi.nlm.nih.gov/datasets/genome/GCF_015227675.2/
Targeted metabolomics and conventional analyte data	Metabolomics Workbench, NIH	Study ID ST003647 https://dev.metabolomicsworkbench.org:22222/data/DRCCMetadata.php?Mode=Study&StudyID=ST003647&Access=RixQ8335 DOI: https://doi.org/10.21228/M8WC2H
Experimental models: Organisms/strains		
Obese Prone CD (OP/CD) Sprague-Dawley rats: Crl:OP(CD), Males	Gifts from Drs. Warren Grill and Eric Gonzalez, Duke University	N/A
Oligonucleotides		
GalNAc-siChREBP 5'CCGACCUUUAUUUGAGUCCU3'	Biosynthesis Inc.	N/A
GalNAc-siCtrl 5'UUCGUACGCGAAUACUUUCGA3'	Biosynthesis Inc.	N/A
Oligonucleotide sequences used for qPCR analyses listed in Table S1	This paper	N/A
Software and algorithms		
Agilent MassHunter Workstation	Agilent quantitative data analysis	https://www.agilent.com/en/product/software-informatics/mass-spectrometry-software/data-analysis/quantitative-analysis
Waters MassLynx	Waters quantitative data analysis	https://www.waters.com/nextgen/us/en/products/informatics-and-software/mass-spectrometry-software/masslynx-mass-spectrometry-software/masslynx-quantitation-applications.html
GraphPad Prism 10	GraphPad	https://www.graphpad.com/
Morpheus	Broad Institute	https://software.broadinstitute.org/morpheus
QuantStudio Real-Time PCR Software 1.3	Applied Biosystems by Thermo Fisher Scientific	https://www.thermofisher.com/us/en/home/global/forms/life-science/quantstudio-6-7-flex-software.html
Kallisto 0.46.1	Bray et al. ⁴⁸	https://pachterlab.github.io/kallisto/
R 4.3.1	N/A	https://www.r-project.org/
DESeq2 1.38.0	Love et al. ⁴⁹	https://bioconductor.org/packages/release/bioc/html/DESeq2.html
EnrichR	Kuleshov et al. ⁵⁰	https://maayanlab.cloud/Enrichr/
Other		
Hight fat/Hight Sucrose Diet	Research Diets	D12451i

EXPERIMENTAL MODEL AND STUDY PARTICIPANT DETAILS

Administration of GalNAc-siRNA reagents and testing during survival period

Breeding pairs of Obese Prone CD (OP/CD) Sprague-Dawley rats were gifts from Dr. Warren Grill and Dr. Eric Gonzalez, Duke University, and a colony was established and maintained by Duke Laboratory Animal Resources (DLAR). Starting at 4 weeks of age, male OP/CD rats were single-housed with a light cycle of 7 a.m. on/7 p.m. off, and fed *ad libitum* with a high-fat/high-sucrose (HF/HS) diet (D12451i, Research Diets) containing 47% fat (kcal) and 17% sucrose (kcal). Body weight and food intake were monitored weekly. After 9 weeks of feeding of the HF/HS diet, plasma samples were collected via saphenous vein bleeding. One week later, animals received an initial subcutaneous injection of one of two GalNAc-siRNA constructs (GalNAc-siChREBP or GalNAc-siCtrl) at a dose of 9 mg/kg body weight, or an equal volume of the diluent (PBS), (see below for description of the two GalNAc-siRNA reagents). Additional doses of 9 mg/kg of each GalNAc-siRNA construct or saline were injected at 10, 18 and 25 days after the first injection. Animals were fasted overnight one day after the third injection (day 19), and subjected to an intraperitoneal glucose tolerance test (IPGTT) on

the following day. Animals were weighed and a glucose solution (1 g/kg body weight) was administered via intraperitoneal injection. Tail blood samples were obtained and glucose levels measured with a blood glucose meter (CVSHealth) immediately before and at 30, 60, 90, 120, and 180 min after bolus injection of glucose. One day after the fourth GalNAc-siRNA or saline injection on day 25, plasma samples were collected via saphenous vein bleeding. A bolus of deuterium oxide (D_2O , 10 mL/kg body weight, Sigma Aldrich) was then given by intraperitoneal injection, followed by free access to drinking water supplemented with 4% D_2O for the rest of the experimental period. Saphenous plasma samples were collected again one day after the bolus delivery of D_2O (day 27).

Tissue harvesting procedure

On day 28 between 8 a.m. and noon, animals were anesthetized and sacrificed for collection of plasma and tissue samples. To minimize tissue harvest time, a team of 3 scientists collected tissues from the animals via the following procedure. Animals were anesthetized with 250 mg/kg Nembutal, and the abdomen and diaphragm were surgically opened. Five mL of blood was drawn from the heart, and one operator centrifuged the sample, collected the plasma, and transferred it to Eppendorf tubes for rapid freezing by submersion in liquid nitrogen. The other two team members proceeded to immediate surgical excision of the heart and liver, which were briefly rinsed with ice-cold PBS, quickly wrapped in aluminum foil, and then frozen by submersion in liquid nitrogen. The time elapsed between beginning of surgery to removal and freezing of the heart and liver was less than 2 min. Other tissues (skeletal muscle, adipose, kidney) were collected after excision of the heart and liver and rapidly frozen in liquid nitrogen. All tissues were stored at -80°C until processing for metabolomic, transcriptomic, and proteomic analyses. To prepare samples for analyses, frozen livers were pulverized under liquid nitrogen, and weighed aliquots of the powder (50 mg powdered tissue/aliquot) was transferred into pre-frozen Eppendorf tubes and extracted for metabolic analyses in 950 μL of extraction buffer. Extraction buffers used for various metabolite modules were: 1) 50% acetonitrile/0.3% formic acid for the amino acid, acylcarnitine, organic acid, creatine, phosphocreatine, creatinine, and guanidinoacetate measurements; 2) 100% methanol for the nucleotide analyses; 3) 3M perchloric acid for the branched-chain keto acid analyses, and 4) 0.3M perchloric acid for the short-chain acyl-CoA analyses.

In this study, we included 6 animals in the GalNAc-siChREBP group, 5 animals in the GalNAc-siCtrl group, and 5 animals in the saline group. We noted at the time of sacrifice, one animal in the GalNAc-siCtrl group died while under anesthesia just prior to organ harvest. We decided to exclude this animal from the post-harvest metabolite analyses based on our observation that it produced multiple tissue metabolite levels that were two or more standard deviations from the population mean. No other animals in the GalNAc-siCtrl or any other group contained such metabolite outliers. This same animal was not an outlier with respect to liver RNA analyses, as might be expected given the greater stability of RNA relative to intermediary metabolites, and thus was retained in the RNA-seq and qPCR data.

Approval of animal studies

All procedures were approved by Duke University Institutional Animal Care and Use Committee and performed according to the regulations of the committee.

METHOD DETAILS

Measurement of hepatic triglycerides and glycogen

Hepatic glycogen content was measured as described previously.²⁶ Hepatic triglyceride content was measured using a Triglyceride Liquidcolor kit (StanBio) after chloroform/methanol extraction.²⁶

Construction of GalNAc-siRNAs

GalNAc-siRNA reagents were prepared by Biosynthesis Inc. Each of the siRNA constructs was fully synthesized with standard 2' modified nucleotides. Primetech TEG-GalNAc was conjugated on the 3' end of the sense strand. Individual strands were dual HPLC purified and analyzed by mass spectrometry to verify purity of >98% before annealing the sense and antisense strands as duplexes. The specific siRNA sequences used were: 5'CCGACCUUUAUUUGAGUCU3', specific for ChREBP (si-ChREBP) and 5'UUCGUACGCGGAAUCUUUCGA3', as a non-targeting control siRNA sequence (si-Ctrl).

Metabolomic analyses

Amino acids and acylcarnitines were analyzed by flow injection electrospray ionization tandem mass spectrometry and quantified by isotope or pseudo-isotope dilution using methods described previously.^{12,31} Levels of free coenzyme A (CoA) and short chain acyl-CoAs were assayed by a previously described targeted tandem mass spectrometry method^{30,51} A panel of nucleotides, nicotinamide dinucleotide and purine pathway intermediates were measured by a previously described targeted LS/MS method.³⁷ Chromatographic separations and mass spec analysis were performed using a Xevo TQ-XS quadrupole mass spectrometer coupled to Acquity UPLC system (Waters, Milford, MA) and a Chromolith FastGradient RP-18e 50-2mm column (EMD Millipore, Billerica, MA, USA), and samples were spiked with a cocktail of 9 stable isotope-labeled standards to facilitate analyte quantification. Branched-chain keto acids (BCKA) were analyzed by LC-MS/MS as previously described, using isotopically labeled internal standards KIC-d3, KIV-5C13 (Cambridge Isotope Laboratories), and KMV-d8 (Toronto Research Chemicals).³⁰ Creatine, phosphocreatine, creatinine, and guanidinoacetate were analyzed by LC-MS/MS as described previously.⁵² Metabolite concentrations were computed using an external

calibration constructed from a serial dilution of authentic standards in dialyzed fetal bovine serum (Sigma, MO, USA). Finally, a panel of TCA cycle intermediates/organic acids were measured by targeted GC/MS analysis as described.³¹ All of the metabolomic data obtained is summarized for each individual rat in the study in [Data S5](#), and is also uploaded to the NIH Common Fund's National Metabolomics Data Repository (NMDR) website, the Metabolomics Workbench,⁵³ <https://www.metabolomicsworkbench.org> where it has been assigned Study ID ST003647. The data can be accessed directly via its Project DOI: <https://doi.org/10.21228/M8WC2H>.

Conventional metabolites and hormones

Insulin in rat plasma was measured with an ELISA assay from Meso Scale Discovery (MSD, Rockville, MD). Other analytes were measured on a Beckman DxC 600 analyzer using reagents from Beckman (Brea, CA) for glucose, triglycerides, and AST, and Fujifilm Wako (Osaka, Japan) for non-esterified fatty acids (NEFA), total ketones, and 3-hydroxybutyrate. All of the conventional metabolite and hormone data obtained is summarized for each individual rat in the study in [Data S5](#), and is also uploaded to Metabolomics Workbench, Study ID ST003647.

Measurement of hepatic *de novo* lipogenesis

De novo lipogenesis was measured by $^2\text{H}_2\text{O}$ labeling of newly synthesized fatty acids in the liver using previously described methods.^{12,16} To check for enrichment of D₂O in plasma water, 10 µL plasma was extracted with acetone/acetonitrile solution (1/20, volume ratio) followed by chloroform treatment and used for Gas Chromatography-Mass Spectrometry (GC-MS) analysis with an Agilent 5973N-MSD instrument equipped with an Agilent 6890 GC system, and a DB-17MS capillary column (30 m × 0.25 mm × 0.25 µm). The mass spectrometer was operated in the electron impact mode (EI; 70 eV). The temperature program was as follows: 60°C initial, increase by 20°C/min to 100°C, increase by 50°C/min to 220°C, and hold for 1 min. The sample was injected at a split ratio of 40:1 with a helium flow of 1 mL/min. Acetone eluted at 1.5 min. Total palmitic acid labeling in the liver was assayed by GC-MS. Briefly, 20 mg liver tissue was homogenized in 1 mL KOH/EtOH (EtOH 75%) and incubated at 85°C for 3 h, and 20 µL of 10 mM [D₃₁]palmitate was added to samples as internal standard after cool down. Extracted palmitic acid was mixed with 100 µL N-*tert*-Butyldimethylsilyl-N-methyltrifluoroacetamide (TBDMS) at 70°C for 20 min, and the TBDMS-derivatized samples were analyzed with an Agilent 5973N-MSD equipped with an Agilent 6890 GC system, and a DB-17MS capillary column (30 m × 0.25 mm × 0.25 µm). The mass spectrometer was operated in the electron impact mode (EI; 70 eV). The sample was injected at a split ratio of 10:1 with a helium flow of 1 mL/min. Palmitate-TBDMS derivative eluted at 9.7 min, and the m/z at 313, 314, and 319 were extracted for M0, M1, ..., and up to M16 palmitate quantification. After correction for natural isotope abundance⁵⁴ newly synthesized palmitic acid was calculated as: % newly synthesized palmitic acid labeling = total palmitic acid labeling/(plasma $^2\text{H}_2\text{O}$ labeling × 22) × 100. Plasma D₂O labeling was approximately 1.6% in our study. Labeling of most metabolites remains below 5% at this level of D₂O enrichment, even for metabolites with three exchangeable hydrogens (3 × 1.6%), and M2 labeling is even lower (1.6 × 1.6/100 × 0.984 × 3 = 0.076%). Therefore, labeled metabolites other than newly synthesized fatty acids are largely undetectable in our analyses and do not contribute to errors in measurement of metabolites by targeted mass spectrometry.

Immunoblotting

Frozen liver tissue was lysed in RIPA buffer (150 mM NaCl, 50 mM Tris (pH 8.0), 0.1% SDS, 1% Triton X-100, 0.5% C₂₄H₃₉NaO₄) with complete EDTA-free protease inhibitor cocktail (Roche) and PhosSTOP phosphatase inhibitor cocktail (Roche). 20 µg of protein were resolved by SDS-PAGE and transferred onto PVDF membranes. Membranes were blocked and probed with antibodies. Primary antibodies used were: Phospho-S293-BCKDHA (Abcam ab200577), BCKDH-E1α (CST 90198), Phospho-S454/455-ACLY (CST 4331), ACLY (CST 4332), BCKDK (Abcam ab128935), Vinculin (CST 4650), ChREBP (Novus NB400-135), and TM6SF2 antibody (pAb-505E, a gift from Dr. Helen Hobbs, UT Southwestern Medical Center, Dallas).²⁰ Secondary antibodies used were: IRDye 800CW Donkey Anti-Rabbit IgG and IRDye 680RD Goat Anti-Mouse IgG (Li-Cor). Immunoblots were developed using a Li-Cor Odyssey CLx and quantified using the Li-Cor software.

RNA isolation and qPCR analysis

RNA from rat livers was isolated using TRI Reagent (MilliporeSigma, T9424). RNA was reverse transcribed using a SuperScript VILO MasterMix (Invitrogen, Thermo Fisher Scientific). Gene expression was analyzed using QuantStudio 6 Flex Real-Time PCR System (Applied Biosystems, Thermo Fisher Scientific) and SYBR Green chemistry (PowerUp SYBR Green Master Mix; Applied Biosystems, Thermo Fisher Scientific). Gene-specific primers were synthesized by Thermo Fisher Scientific or MilliporeSigma, and a list of primers used is provided in [Table S1](#). Each sample was run in duplicate. Beta-2-Microglobulin (*B2m*) and TATA-box binding (*Tbp*) transcripts was used as house-keeping genes to normalize expression levels for genes of interest.

RNA sequencing and analysis

RNA was isolated from rat liver with TRI Reagent (MilliporeSigma, T9424). RNA-seq was performed by Novogene, CA. Briefly, mRNA was purified from total RNA using poly-T oligo-attached magnetic beads. After fragmentation, the first strand cDNA was synthesized using random hexamer primers, followed by the second strand cDNA synthesis using dUTP. A directional library was constructed, which included end repair, A-tailing, adapter ligation, size selection, USER enzyme digestion, amplification, and purification. 150 bp paired-end sequencing was performed on an Illumina NovaSeq 6000, and at least 77 million clean reads were obtained per sample.

Pseudoalignment and quantification of transcripts was performed using Kallisto (0.46.1) with a transcript index built from rat genome assembly mRatBN7.2.⁴⁸ Differential gene expression analysis was performed in R (4.3.1) using DESeq2 (1.38.0).⁴⁹ Gene set enrichment analysis was performed using EnrichR.⁵⁰ The raw and processed RNA-seq data corresponding to Data S3 has been deposited to the GEO database (GSE282614). We note that the transcript encoding vinculin, a protein used as an internal control in our immunoblot studies, was not affected by GalNac-siChREBP treatment.

QUANTIFICATION AND STATISTICAL ANALYSIS

Statistical analysis performed using one-way ANOVA followed by Tukey test, unpaired t test. Differential gene expression analysis from RNA-seq data was performed using DeSeq2 with correction for multiple comparisons. Exact statistical methods applied and *n* values are specified in figure legends.